On checking dissipativity of parameterized linear and time-invariant circuits and systems

Received: Added at production | Revised: Added at production | Accepted: Added at production

DOI: 10.1002/cta.3516

ARTICLE TYPE

On checking dissipativity of parameterized LTI circuits and systems

Alessandro Zanco* | Stefano Grivet-Talocia

[1]Department of Electronic and Telecommunications, Politecnico di Torino, Italy

Correspondence
*Corresponding author Alessandro Zanco.
Email: alessandro.zanco@polito.it

Summary

A novel dissipativity characterization is proposed for linear time-invariant circuits and systems whose dynamic behavior depends on one external parameter. The proposed formulation extends to the parameterized case standard Hamiltonian-based algebraic dissipativity characterizations, and is structured as an underdetermined multi-parameter eigenvalue problem. Resulting from a polynomial parameterization, the proposed characterization leads to an effective set of algorithms that are able to determine the regions of local dissipativity and local activity in the frequency-parameter plane, which in turn can be exploited by dissipativity enforcement algorithms to produce uniformly passive models. The reference application of proposed technique is behavioral modeling of complex circuits or systems, whose dynamic behavior can be compressed into a low-order system through dedicated model order reduction processes. Various examples ranging from integrated components to microstrip filters and networks are used to illustrate the proposed characterization.

KEYWORDS:
Dissipativity, Passivity, Model Order Reduction, Behavioral Modeling, Hamiltonian matrices, Skew-Hamiltonian/Hamiltonian pencils, Multiparameter Eigenvalue Problems, Polynomial Eigenvalue Problems.

1 | INTRODUCTION

The focus of this contribution is on Linear and Time-Invariant (LTI) multiport circuit blocks, whose dynamic behavior depends on one external parameter. The latter can be a design variable (e.g. related to geometry of some lumped or distributed component[1]), a material property, or a quantity related to ambient conditions (e.g., temperature[2]). We assume that the underlying circuit or system is dissipative[3] and unable to generate energy on its own. The main objective of this work is to determine whether a mathematical model describing the underlying system is also dissipative, so that the corresponding equations can be safely used in a CAD environment (e.g., a SPICE engine) to reproduce the circuit behavior when inserted as a component within a larger numerical simulation setting. In fact, it is well known that dissipative models provide a guarantee of stable and robust numerical simulation due to their inability to drive system-level simulations to instability. The vice-versa is also true: for any non-dissipative model, there exists a set of loading conditions that are guaranteed to drive the system into instability[4]. This situation is to be avoided.

The reference framework for this contribution is behavioral modeling of complex circuits and systems through Model Order Reduction (MOR)[5], whose reference application scheme is now briefly reviewed. An original large-scale circuit or system is first characterized, leading to some first-principle description of its behavior. This can be in form of Partial Differential Equations

or Integral Equations (PDEs and IEs, e.g. as resulting from Maxwell full-wave formulations), Ordinary Differential Equations (ODEs) or Differential Algebraic Equations (DAEs), the latter being the common choice in circuit formulations based on the Modified Nodal Analysis (MNA), or even in terms of time[6]- or frequency-domain sampled responses[7,8,9,10,11,12]. The latter situation occurs when only direct measurements are available, or alternatively when a non-intrusive solver is used to retrieve the system responses. Irrespective of this first-principle characterization, a plethora of MOR techniques are available to derive compact models that approximate the input-output behavior of the system. For a comprehensive review the Reader is referred to the recent book series[13] and to the references therein.

Compact reduced-order models are a fundamental resource for design engineers in electrical and electronic applications[14], as key enabling factors for those fast numerical simulations that are required for early-stage design and verification. Based on the above considerations, the dissipativity verification of reduced order models is recognized as a crucial step to enable MOR-based CAD flows, thus justifying the huge amount of literature on the subject. As an example, we mention the seminal theoretical works[3,15,16,17] as well as the more application-oriented frameworks, including passivity enforcement algorithms of LTI behavioral representations of circuit blocks[18,19,20,21,22], fractional order systems[23,24], circuit approximations of electromagnetic systems via integral formulations[25] and others[26,27].

When the dynamics of the system under investigation depend on one or more parameters, the problem of enforcing dissipativity (or passivity, both terms are used here as synonyms) in the reduced model is quite challenging. The compact and parameter-dependent system of differential equations resulting from the adopted MOR scheme does not necessarily preserve dissipativity, as a result of the various approximations involved in the reduction process. This fact motivated a consistent research effort towards enforcing dissipativity of parameterized models[8,9,28,29,30,31]. A prerequisite for most of these formulations is the availability of a tool for the verification of the appropriate dissipativity conditions, uniformly in the allowed parameter range. More precisely, a formulation and a related algorithm that is able to determine the regions of local dissipativity and local activity in the frequency-parameter plane would be highly desired, so that this information can be used to setup passivity enforcement algorithms aimed at eliminating the locally active regions and recover uniform dissipativity by model perturbation. Several algorithms for this task are available[29,30,31], the main bottleneck remaining the dissipativity characterization.

This paper presents a novel dissipativity characterization of LTI models in parameterized descriptor form[12]. The proposed formulation extends spectral characterizations of non-parameterized models based on the associated Hamiltonian matrix[20,14] to the bivariate case, allowing dependence of the transfer function on one external parameter in addition to frequency. Based on an orthogonal polynomial parameterization[32], the proposed method leads to an underdetermined multi-parameter eigenvalue problem[33], whose solutions provide the boundaries between locally active and locally dissipative regions. Based on this formulation, an algorithm that discretizes these boundaries along polynomial trajectories in the frequency-parameter plane is presented. Various numerical examples on practical application cases (a microstrip filter and an integrated inductor) show that proposed approach and algorithm are able to produce extremely accurate characterizations with moderate computing requirements.

This paper is structured as follows. Section 2 presents reference background information and introduces notation, in particular the structure of the adopted model equations and related parameterization, as well as global and local dissipativity conditions. Section 3 presents Hamiltonian matrix and Skew Hamiltonian/Hamiltonian pencil spectral characterizations of dissipativity, whereas Section 4 introduces the proposed multi-parameter eigenvalue formulation, including its discretization along polynomial trajectories. Section 5 presents numerical results with applications to practical test cases, and Section 6 draws conclusions.

2 | BACKGROUND AND NOTATION

Let us consider a Linear-Time-Invariant (LTI) and dissipative P-port circuit block, whose behavior depends on a real-valued parameter $\vartheta \in \Theta$, where Θ is a normalized interval. The system is described by a behavioral reduced-order model $\mathcal{S}(\vartheta)$, here assumed in the (parameterized) *descriptor* form[34]

$$\mathcal{S}(\vartheta) : \begin{cases} \mathbf{E}\dot{\mathbf{x}}(t,\vartheta) = \mathbf{A}(\vartheta)\mathbf{x}(t,\vartheta) + \mathbf{B}\mathbf{u}(t) \\ \mathbf{y}(t,\vartheta) = \mathbf{C}(\vartheta)\mathbf{x}(t,\vartheta) \end{cases} \tag{1}$$

where $\mathbf{x}(t,\vartheta) \in X \subset \mathbb{R}^N$ collects the time- and parameter-dependent states, $\mathbf{u}(t) \in U \subset \mathbb{R}^P$ is the vector of system inputs, and $\mathbf{y}(t,\vartheta) \in Y \subset \mathbb{R}^P$ collects the outputs. Without loss of generality, the input matrix $\mathbf{B}$ is assumed constant, and the output parameterization is induced by matrix $\mathbf{C}(\vartheta)$. System dynamics (the natural frequencies) are parameterized through the matrix

$\mathbf{A}(\vartheta)$, with a constant descriptor matrix $\mathbf{E}$. This parameterization structure is general and well-established, see e.g., [7,12,35,1], where a set of algorithms are presented for the construction of a reduced model in form (1) from response data.

We suppose the following properties to hold uniformly throughout the parameter space:

- the pencil $(\mathbf{A}(\vartheta), \mathbf{E})$ is uniformly regular[34], i.e., $\forall \vartheta \in \Theta,\ \exists s \in \mathbb{C} : |s\mathbf{E} - \mathbf{A}(\vartheta)| \neq 0$
- the model $\mathcal{S}(\vartheta)$ is uniformly asymptotically stable, i.e., $\forall \vartheta \in \Theta,\ \Re\{\lambda(\vartheta)\} < 0$ where $\lambda(\vartheta)$ denotes any finite eigenvalue of the pencil $(\mathbf{A}(\vartheta), \mathbf{E})$.

These two conditions are fundamental in applications requiring robust transient simulations. References [1,36,37] provide a framework that guarantees these two conditions by construction. It is therefore possible to define the input-output transfer function of the system

$$\mathbf{G}(s, \vartheta) = \mathbf{C}(\vartheta)(s\mathbf{E} - \mathbf{A}(\vartheta))^{-1}\mathbf{B} \tag{2}$$

which for any $\vartheta \in \Theta$ is regular in the closed half plane $\Re\{s\} \geq 0$.

2.1 | Parameterization through orthogonal polynomials

The dependence of the descriptor matrices on the parameter ϑ is here assumed to be polynomial, although various other types of parameterization have been proposed, such as trigonometric polynomials[38] or radial basis functions[38,1]. Here we assume the general form

$$\mathbf{A}(\vartheta) = \sum_{\ell=0}^{\bar{\ell}} \mathbf{A}_\ell \xi_\ell(\vartheta), \quad \mathbf{C}(\vartheta) = \sum_{\ell=0}^{\bar{\ell}} \mathbf{C}_\ell \xi_\ell(\vartheta) \tag{3}$$

where the basis functions $\xi_\ell(\vartheta)$ are orthogonal polynomials[32] defined on the domain Θ. Orthogonal polynomial bases are well conditioned in numerical processing, while providing excellent approximations of smooth functions, with an accuracy controlled by the expansion order $\bar{\ell}$.

All orthogonal polynomial families are characterized by recurrence relations defining the individual basis elements. For any $\ell > 0$ we have[39]

$$\xi_\ell(\vartheta) = (\alpha_{\ell-1}\vartheta + \beta_{\ell-1})\xi_{\ell-1}(\vartheta) + \delta_{\ell-1}\xi_{\ell-2}(\vartheta) \tag{4}$$

with $\xi_0(\vartheta) = 1$ and $\xi_{-1}(\vartheta) = 1$, and where $\alpha_\ell, \beta_\ell, \delta_\ell$ are real coefficients. For common orthogonal polynomial families defined on a bounded interval, these coefficients read[39]

- Chebychev: $\alpha_{\ell-1} = 2$, $\beta_{\ell-1} = 0$, $\delta_{\ell-1} = -1$
- Legendre: $\alpha_{\ell-1} = (2\ell + 1)/\ell$, $\beta_{\ell-1} = 0$, $\delta_{\ell-1} = -(\ell - 1)/\ell$

2.2 | Dissipative systems

In this work, we are interested in the characterization of the energetic properties of (1), with the main objective of assessing whether the model is dissipative. In fact, although the reference circuit block is known to be dissipative, an order-reduction process does not necessarily preserve this property. If this is the case, and apart from a fundamental inconsistency of the energetic properties of the model, the latter cannot not be safely employed in CAD flows and especially time-domain simulations: depending on the actual loading conditions, a non-dissipative model may lead to unstable results[4].

In this section we recall the notion of dissipativity in order to set the notation for later developments.

2.2.1 | Supply rate

The system exchanges energy and power with the environment through its input and output signals $\mathbf{u}$ and $\mathbf{y}$ (in the following we will omit the dependence on time and parameter variables on vectors $\mathbf{u}(t)$, $\mathbf{y}(t, \vartheta)$ to improve readability). This exchange is best described through a *supply rate*

$$p(\mathbf{u}, \mathbf{y}) : U \times Y \to \mathbb{R} \tag{5}$$

which corresponds to the instantaneous power flow that enters the system at any given time. The dependence of supply rates on input and output vectors is usually quadratic. With reference to lumped or distributed circuit blocks, where input and output signals are port voltages and currents (for immittance representations) or incident and reflected scattering waves (for scattering representations), we have the two following definitions

1. Immittance: $p(\mathbf{u},\mathbf{y}) = \mathbf{u}^\mathsf{T}\mathbf{y}$,
2. Scattering: $p(\mathbf{u},\mathbf{y}) = \mathbf{u}^\mathsf{T}\mathbf{u} - \mathbf{y}^\mathsf{T}\mathbf{y}$

These are just two particular cases a more general *quadratic supply*[40] defined as

$$p(\mathbf{u},\mathbf{y}) = \mathbf{u}^\mathsf{T}\mathbf{Q}\mathbf{u} + 2\mathbf{y}^\mathsf{T}\mathbf{S}^\mathsf{T}\mathbf{u} + \mathbf{y}^\mathsf{T}\mathbf{R}\mathbf{y} = \begin{pmatrix}\mathbf{u}\\ \mathbf{y}\end{pmatrix}^\mathsf{T}\begin{pmatrix}\mathbf{Q} & \mathbf{S}\\ \mathbf{S}^\mathsf{T} & \mathbf{R}\end{pmatrix}\begin{pmatrix}\mathbf{u}\\ \mathbf{y}\end{pmatrix} \tag{6}$$

where $\mathbf{Q}, \mathbf{S}$, and $\mathbf{R}$ are real-valued matrices of size $P \times P$. One can easily verify that the above immittance and scattering cases are recovered by setting $\{\mathbf{Q} = \mathbf{R} = \mathbf{0},\ \mathbf{S} = \frac{1}{2}\mathbf{I}_P\}$, and $\{\mathbf{Q} = \mathbf{I}_P, \mathbf{R} = -\mathbf{I}_P,\ \mathbf{S} = \mathbf{0}\}$, respectively.

2.2.2 | Storage function and dissipation inequality

The power entering the system can be either dissipated or stored in form of internal energy. For the case of electrical networks, this energy is stored in charged capacitors and inductors through their voltages and currents, which collectively represent the state variables. For a reduced-order model (1), the state variables $\mathbf{x}$ may not necessarily represent physical circuit elements, since derived from a model order reduction process, and should be regarded as abstract states.

The energy stored in the system is usually characterized by a *storage function*

$$V(\mathbf{x}) : X \to \mathbb{R}. \tag{7}$$

For dissipative systems, the energy that is incrementally stored during any interval $[t_1, t_2]$ cannot exceed the cumulative amount of power received by the system during this interval. In the considered case of parameterized systems, the concept of uniform dissipativity is of interest, for which this condition must hold for any parameter configuration. Therefore, we consider the following[3]:

Definition 1. *Uniform Dissipativity*
A parameterized system (1) described by the supply rate $p(\mathbf{u}(t), \mathbf{y}(t,\vartheta))$ is *uniformly dissipative* if and only if there exists a storage function $V(\mathbf{x}(t,\vartheta))$ such that

$$V(\mathbf{x}(t_2,\vartheta)) \leq V(\mathbf{x}(t_1,\vartheta)) + \int_{t_1}^{t_2} p(\mathbf{u}(t), \mathbf{y}(t,\vartheta))dt \tag{8}$$

for all $\vartheta \in \Theta$, for all $t_1 \leq t_2$ and for all the combinations of input $\mathbf{u}(t)$, output $\mathbf{y}(t,\vartheta)$ and state variables $\mathbf{x}(t,\vartheta)$ which satisfy (1).

For LTI systems, the storage function $V(\mathbf{x}(t,\vartheta))$ is guaranteed to exist and it comes as a quadratic function of the system states $\mathbf{x}(t,\vartheta)$[41,40].

2.2.3 | Frequency domain characterization

A characterization of dissipative LTI systems can be provided in various equivalent forms. Here, we will not consider algebraic characterizations in terms of Linear Matrix Inequalities (LMIs) such as the Kalman-Yakubovich-Popov (KYP) lemma in its various declinations, and we will focus on frequency-domain and Hamiltonian matrix characterizations. The Reader is referred to References[17,40,42,43] for a complete theoretical framework.

It can be shown[40] that the dissipation inequality (8) translates into an equivalent frequency-domain matrix inequality condition. In particular, a LTI system described by the transfer function $\mathbf{G}(s,\vartheta)$ and equipped with the quadratic supply rate (6) is uniformly dissipative if and only if

$$\mathbf{\Psi}(s,\vartheta) \succeq 0, \quad \forall s \in \mathbb{C}^+,\ \vartheta \in \Theta \tag{9}$$

where $\mathbf{\Psi}(s,\vartheta) : \mathbb{C}^+ \times \Theta \to \mathbb{C}^{P\times P}$ is defined as

$$\mathbf{\Psi}(s,\vartheta) = \begin{pmatrix}\mathbf{I}\\ \mathbf{G}(s,\vartheta)\end{pmatrix}^\dagger\begin{pmatrix}\mathbf{Q} & \mathbf{S}\\ \mathbf{S}^\mathsf{T} & \mathbf{R}\end{pmatrix}\begin{pmatrix}\mathbf{I}\\ \mathbf{G}(s,\vartheta)\end{pmatrix} \tag{10}$$

where $(\cdot)^\dagger$ denotes the conjugate transpose of its matrix argument.

In our particular case of uniformly asymptotically stable systems, the transfer matrix $\mathbf{G}(s,\vartheta)$ is well-defined and regular on the imaginary axis $s = \mathrm{j}\omega$. Therefore, the above dissipativity condition can be equivalently restricted to the imaginary axis only as

$$\mathbf{\Psi}(\mathrm{j}\omega,\vartheta) \succeq 0, \quad \forall \omega \in \mathbb{R},\ \vartheta \in \Theta. \tag{11}$$

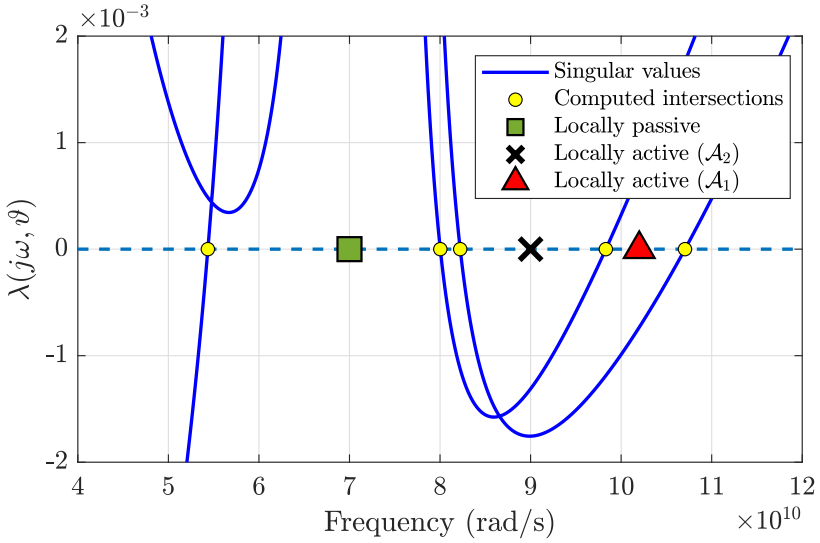

Figure 1 Illustration of local activity and local dissipativity of a system with $P = 2$ ports. Assuming a fixed $\vartheta = \vartheta_0$, the blue trace depicts the trajectory of the smallest eigenvalue $\lambda(\mathrm{j}\omega, \vartheta_0) = \min\{\Lambda(\mathrm{j}\omega, \vartheta_0)\}$. The system is locally dissipative (green square marker) when $\lambda > 0$ and locally active (black cross marker) when at least one $\lambda < 0$. The transitions between locally dissipative and locally active regions (or between two locally active with a mutually different number of negative eigenvalues) are highlighted with yellow filled dots.

Standard arguments are available for proving (11) based on (9) if asymptotic stability holds[17,44].

The condition (11) characterizes dissipative systems, for which all eigenvalues $\lambda(\mathrm{j}\omega, \vartheta)$ of matrix $\boldsymbol{\Psi}(\mathrm{j}\omega, \vartheta)$ are nonnegative in $\mathbb{R} \times \Theta$. When this condition is violated, a *local* characterization can be carried out, by splitting the frequency-parameter domain into disjoint regions where the system behaves as dissipative or non-dissipative. Defining as $\Lambda(\mathrm{j}\omega, \vartheta)$ the set of P eigenvalues of $\boldsymbol{\Psi}(\mathrm{j}\omega, \vartheta)$, we denote the system at a given fixed $(\mathrm{j}\omega, \vartheta)$ as

- *locally strictly dissipative* if $\lambda > 0, \ \forall \lambda \in \Lambda(\mathrm{j}\omega, \vartheta)$;
- *locally active* if $\exists \lambda \in \Lambda(\mathrm{j}\omega, \vartheta)$ such that $\lambda < 0$.

Figure 1 provides a graphical illustration.

We collect all points where the system behaves as locally dissipative in the set

$$\mathcal{D} = \{(\mathrm{j}\omega, \vartheta) : \lambda > 0, \ \forall \lambda \in \Lambda(\mathrm{j}\omega, \vartheta)\} \tag{12}$$

whereas we define the set with locally active points

$$\mathcal{A} = \{(\mathrm{j}\omega, \vartheta) : \exists \lambda < 0 \text{ and } \forall \lambda \neq 0, \ \lambda \in \Lambda(\mathrm{j}\omega, \vartheta)\}. \tag{13}$$

Note that any point at which the matrix $\boldsymbol{\Psi}(\mathrm{j}\omega, \vartheta)$ becomes singular with a vanishing eigenvalue is excluded from the above two sets. Such points are collected in a third set

$$\mathcal{Z} = \{(\mathrm{j}\omega, \vartheta) : \exists \lambda = 0, \ \lambda \in \Lambda(\mathrm{j}\omega, \vartheta)\}. \tag{14}$$

We thus have a complete partition $\mathrm{j}\mathbb{R} \times \Theta = \mathcal{D} \cup \mathcal{A} \cup \mathcal{Z}$, where the three subsets are mutually disjoint.

The set of locally active points can be further split into mutually disjoint subsets

$$\mathcal{A} = \mathcal{A}_1 \cup \mathcal{A}_2 \cup \cdots \cup \mathcal{A}_P \tag{15}$$

where each subset $\mathcal{A}_i$ is characterized by an exact number i of negative eigenvalues in $\Lambda(\mathrm{j}\omega, \vartheta)$, with the remaining $P - i$ eigenvalues being strictly positive. Note that the set $\mathcal{Z}$ provides the boundaries of the sets $\mathcal{D}$ and $\mathcal{A}_i$. See Fig. 2 for a graphical illustration.

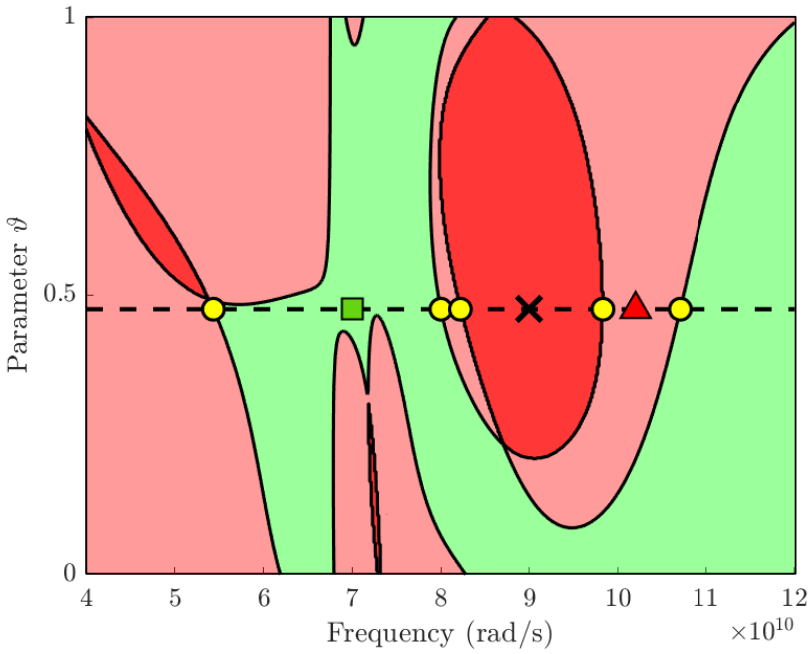

Figure 2 Subdivision of the frequency-parameter space based on the number of negative eigenvalues λ: the locally dissipative set $\mathcal{D}$ is depicted with a light green, while the locally active regions $\mathcal{A}_i$ are represented with increasingly strong shades of red: in this particular example, the sets $\mathcal{A}_1$ and $\mathcal{A}_2$ correspond to light and strong hues, respectively. The horizontal line corresponds to sectioning the space $\mathrm{j}\mathbb{R} \times \Theta$ with a constant parameter value: the transitions between different regions along this line are highlighted with yellow filled dots; these transitions correspond to the zero-crossing of the eigenvalue in Fig. 1.

.

2.2.4 | Why local characterization?

The objective of this work is to provide a novel theoretical representation and an algorithmic procedure for the classification of the frequency-parameter space into locally dissipative and active regions, so that all sets $\mathcal{D}$, $\mathcal{A}_i$ and their boundaries $\mathcal{Z}$ are identified. The motivation for this investigation is induced by the requirement that reduced-order behavioral models (1) must be uniformly dissipative in order to be safely used in system-level simulations and CAD flows. Whenever locally active regions $\mathcal{A}_i$ are present, the model must be adjusted through a suitable perturbation approach so that the resulting system satisfies the uniform dissipativity conditions (11). Passivity (dissipativity) enforcement based on local eigenvalue perturbation constraints formulated on locally active regions is a well established and well documented technique, which is not discussed in this work. We refer the Reader to [19,45,20,46,47] for an overview of passivity enforcement methods for non-parameterized systems and to the more recent works [36,30,48] for generalization to the parameterized case. All common perturbation-based passivity enforcement schemes require in their initial setup some local characterization for setting up appropriate constraints.

3 | CHARACTERIZATION THROUGH HAMILTONIAN MATRICES AND PENCILS

Characterization through Hamiltonian matrices is the standard method for assessing the dissipativity of regular (non-parameterized) state-space systems [20]. Hamiltonian matrices provide an effective algebraic approach to detect the frequencies at which the system switches from locally dissipative to locally active. Such frequencies are identified by the purely imaginary eigenvalues of the Hamiltonian matrices.

Generalizations to descriptor systems require Skew-Hamiltonian/Hamiltonian (SHH) pencils [49,50,51], which are also well established. Extension to the parameterized case has also been proposed, and several techniques based on sampling have been introduced for the identification of locally active regions [30,31]. Since based on sampling, all presented approaches are prone to miss locally active regions, which is a serious limitation.

In this work, we provide an alternative characterization for the local dissipativity properties of parameterized systems (1), by introducing a multivariate linear eigenvalue problem arising from a Hamiltonian matrix approach. This representation enables new approaches for sampling the frequency-parameter space, which have the potential of providing more uniform coverage hence reliability in detecting locally active regions.

3.1 | Spectral dissipativity characterization

The objective of this section is to derive equivalent algebraic conditions defining the set $\mathcal{Z}$, which collects all the points $(\mathrm{j}\omega, \vartheta)$ where one of the eigenvalues of $\mathbf{\Psi}(\mathrm{j}\omega, \vartheta)$ vanishes. This condition occurs if there exists a non-zero vector $\mathbf{v}$ such that

$$\mathbf{\Psi}(\mathrm{j}\omega, \vartheta) \cdot \mathbf{v} = \mathbf{0}. \tag{16}$$

Let us write the matrix function $\mathbf{\Psi}(\mathrm{j}\omega, \vartheta)$ by expanding the product (10), as

$$\mathbf{\Psi}(\mathrm{j}\omega, \vartheta) = \mathbf{Q} + \mathbf{S}\mathbf{G}(\mathrm{j}\omega, \vartheta) + \mathbf{G}(\mathrm{j}\omega, \vartheta)^{\dagger}\mathbf{S}^{\mathsf{T}} + \mathbf{G}(\mathrm{j}\omega, \vartheta)^{\dagger}\mathbf{R}\mathbf{G}(\mathrm{j}\omega, \vartheta)$$

Defining the auxiliary vectors

$$\begin{aligned} \mathbf{r} &= [\mathrm{j}\omega\mathbf{E} - \mathbf{A}(\vartheta)]^{-1}\mathbf{B}\mathbf{v} \\ \mathbf{q} &= [-\mathrm{j}\omega\mathbf{E}^{\mathsf{T}} - \mathbf{A}(\vartheta)^{\mathsf{T}}]^{-1}[\mathbf{C}(\vartheta)^{\mathsf{T}}\mathbf{S}^{\mathsf{T}}\mathbf{v} + \mathbf{C}(\vartheta)^{\mathsf{T}}\mathbf{R}\mathbf{C}(\vartheta)\mathbf{r}] \end{aligned} \tag{17}$$

and combining with (16), (17) and (2) leads to the following system

$$\begin{cases} \mathrm{j}\omega\mathbf{E}\mathbf{r} = \mathbf{A}(\vartheta)\mathbf{r} + \mathbf{B}\mathbf{v} \\ \mathrm{j}\omega\mathbf{E}^{\mathsf{T}}\mathbf{q} = -\mathbf{C}(\vartheta)^{\mathsf{T}}\mathbf{R}\mathbf{C}(\vartheta)\mathbf{r} - \mathbf{A}(\vartheta)^{\mathsf{T}}\mathbf{q} - \mathbf{C}(\vartheta)^{\mathsf{T}}\mathbf{S}^{\mathsf{T}}\mathbf{v} \\ \mathbf{S}\mathbf{C}(\vartheta)\mathbf{r} + \mathbf{B}^{\mathsf{T}}\mathbf{q} + \mathbf{Q}\mathbf{v} = \mathbf{0} \end{cases} \tag{18}$$

The quadratic term $\mathbf{C}(\vartheta)^{\mathsf{T}}\mathbf{R}\mathbf{C}(\vartheta)$ in the second equation can be eliminated by introducing an additional auxiliary vector $\mathbf{w} = \mathbf{R}\mathbf{C}(\vartheta)\mathbf{r}$, obtaining a system with a linear dependence on all descriptor matrices

$$\begin{cases} \mathrm{j}\omega\mathbf{E}\mathbf{r} = \mathbf{A}(\vartheta)\mathbf{r} + \mathbf{B}\mathbf{v} \\ \mathrm{j}\omega\mathbf{E}^{\mathsf{T}}\mathbf{q} = -\mathbf{C}(\vartheta)^{\mathsf{T}}\mathbf{w} - \mathbf{A}(\vartheta)^{\mathsf{T}}\mathbf{q} - \mathbf{C}(\vartheta)^{\mathsf{T}}\mathbf{S}^{\mathsf{T}}\mathbf{v} \\ \mathbf{w} = \mathbf{R}\mathbf{C}(\vartheta)\mathbf{r} \\ \mathbf{S}\mathbf{C}(\vartheta)\mathbf{r} + \mathbf{B}^{\mathsf{T}}\mathbf{q} + \mathbf{Q}\mathbf{v} = \mathbf{0} \end{cases} \tag{19}$$

Collecting these equations in a compact matrix form reveals a generalized eigenvalue problem

$$\mathbf{M}(\vartheta) \cdot \mathbf{k} = \mathrm{j}\omega\mathbf{Y} \cdot \mathbf{k} \tag{20}$$

where

$$\mathbf{M}(\vartheta) = \begin{pmatrix} \mathbf{A}(\vartheta) & \mathbf{0} & \mathbf{B} & \mathbf{0} \\ \mathbf{0} & -\mathbf{A}(\vartheta)^{\mathsf{T}} & -\mathbf{C}(\vartheta)^{\mathsf{T}}\mathbf{S}^{\mathsf{T}} & -\mathbf{C}^{\mathsf{T}} \\ \mathbf{S}\mathbf{C}(\vartheta) & \mathbf{B}^{\mathsf{T}} & \mathbf{Q} & \mathbf{0} \\ \mathbf{R}\mathbf{C}(\vartheta) & \mathbf{0} & \mathbf{0} & -\mathbf{I}_P \end{pmatrix} \tag{21}$$

$$\mathbf{Y} = \begin{pmatrix} \mathbf{E} & \mathbf{0} & \mathbf{0} & \mathbf{0} \\ \mathbf{0} & \mathbf{E}^{\mathsf{T}} & \mathbf{0} & \mathbf{0} \\ \mathbf{0} & \mathbf{0} & \mathbf{0} & \mathbf{0} \\ \mathbf{0} & \mathbf{0} & \mathbf{0} & \mathbf{0} \end{pmatrix}, \qquad \mathbf{k} = \begin{pmatrix} \mathbf{r} \\ \mathbf{q} \\ \mathbf{v} \\ \mathbf{w} \end{pmatrix} \tag{22}$$

where $\mathbf{M}(\vartheta)$ and $\mathbf{Y}$ are square with dimensions $2(P+N)$. The (generalized) eigenvalue of this pencil is $\mathrm{j}\omega$ with the corresponding eigenvector $\mathbf{k}$.

Note that (20) is just a reformulation of (16). Therefore, if a purely imaginary eigenvalue $\mathrm{j}\omega$ is found, the corresponding frequency/parameter combination $(\mathrm{j}\omega, \vartheta)$ is concluded to belong to $\mathcal{Z}$. Considering the parameter ϑ as frozen, and collecting all (sorted) frequencies of imaginary eigenvalues in the set $\Omega = \{\omega_1, \omega_2, \dots\}$, we see that Ω provides a partition of the frequency axis into disjoint frequency bands (ω_j, ω_{j+1}) where the number of negative eigenvalues of $\mathbf{\Psi}(\mathrm{j}\omega, \vartheta)$ is constant. If this number is zero, the corresponding band is locally dissipative, otherwise it is locally active. Freezing ϑ corresponds to sectioning the strip $j\mathbb{R} \times \Theta$ with a horizontal line, as in Fig. 2.

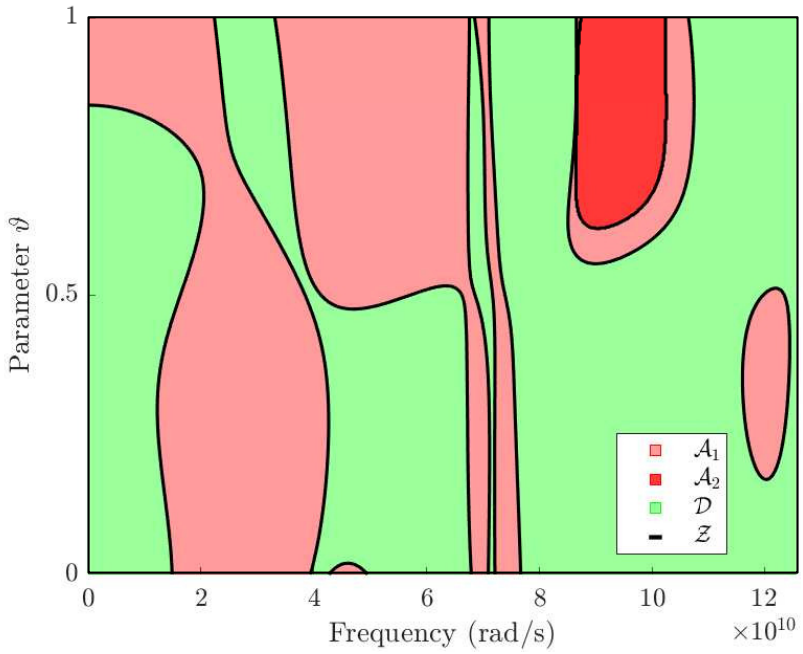

Figure 3 Frequency-parameter plane partitioned into locally dissipative ($\mathcal{D}$, green) and locally active ($\mathcal{A}_i$, shades of red) areas, separated by the boundary $\mathcal{Z}$.

The above characterization is well known[52] and has been exploited in various software suites for passivity characterization and enforcement. Although the pencil (20) does not have a particular structure, under particular cases it is possible to eliminate some of the auxiliary vectors used in the above derivations, leading to a pencil (matrix) with SHH (Hamiltonian) structure. This structure is not essential for the following derivations, although it may be convenient for robust numerical evaluation of the eigenvalues, since the underlying Hamiltonian structure implies a symmetry of the eigenvalue spectrum with respect to both real and imaginary axes. Specialized eigensolvers are available for exploiting such symmetry[53].

4 | MULTI-PARAMETER EIGENVALUE FORMULATION

The algebraic structure of the eigenvalue problem (20) shows that frequency ω and external parameters ϑ play different roles. While frequency appears as an eigenvalue, the parameter ϑ is only implicitly accounted for through the dependence of the individual descriptor matrices. In this section, we show that for the particular case of (orthogonal) polynomial dependence, system (20) can be rewritten in an equivalent form where also ϑ plays the role of an eigenvalue.

We state below the main result without proof. The derivations providing a detailed proof are tedious but straightforward and are reported in the Appendix A. We have the following

Theorem 1. Consider a descriptor system (1) with parameterization defined as in (3) where $\xi_\ell(\vartheta)$ are orthogonal polynomials characterized by recurrence relations (4). Then, $\mathbf{\Psi}(\mathrm{j}\omega, \vartheta)$ is singular if and only if there exists a non-zero vector $\mathbf{z}$ such that

$$(\mathbf{P}_0 + \vartheta \mathbf{P}_1 - \mathrm{j}\omega \mathbf{J}) \cdot \mathbf{z} = \mathbf{0} \tag{23}$$

where $\mathbf{P}_0,\ \mathbf{P}_1,\ \mathbf{J}$ are constant real-valued square matrices (defined in Appendix A) of dimension $2\bar{\ell}(N+P)$.

The formulation (23), which is equivalent to (20) for the assumed class of systems, can be considered as an incomplete or underdetermined multi-parameter eigenvalue problem[33,54]. The set of all points $(\mathrm{j}\omega, \vartheta)$ that satisfy (23) defines set $\mathcal{Z}$. Under a topological standpoint, this set can be represented as a union of curves in the plane (ω, ϑ). Such curves can be closed or open, and they can even cross each other, leading to an overall non-smooth behavior. Some examples are provided in Fig. 3.

We have already discussed the standard spectral characterization for fixed ϑ, which provides the intersection of $\mathcal{Z}$ with a line $\vartheta = \vartheta_0$. The formulation (23) enables the dual case of freezing the frequency value in order to find the intersections of $\mathcal{Z}$ with

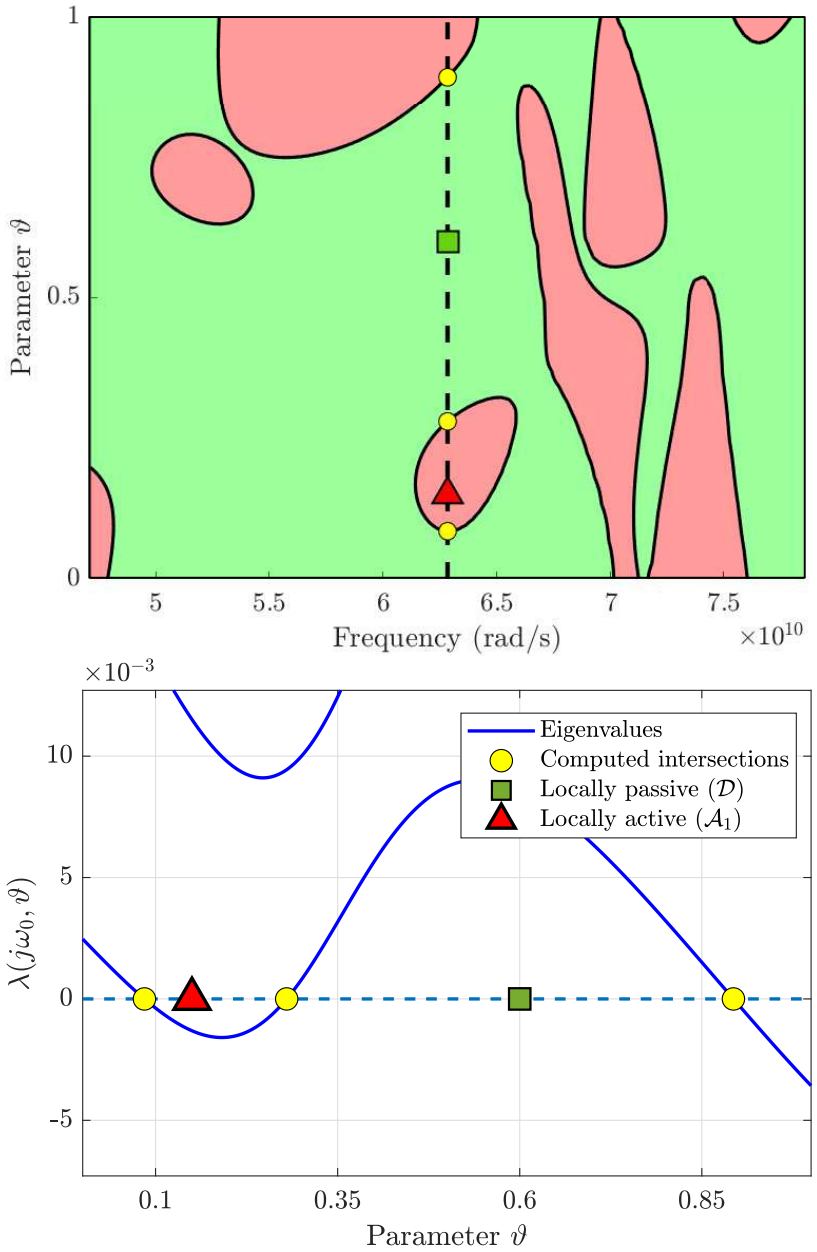

Figure 4 Localization of the transitions between locally active and locally dissipative regions along a vertical cut (fixed frequency), performed through (24). Top panel: frequency-parameter plane; bottom panel: trajectory of parameter-dependent eigenvalues $\lambda(\mathrm{j}\omega_0, \vartheta)$.

a line $\omega = \omega_0$. These intersections are computed as the generalized eigenvalues $\vartheta \in \Theta$ of

$$(\mathbf{P}_0 - \mathrm{j}\omega_0 \mathbf{J}) \cdot \mathbf{z} = -\vartheta\, \mathbf{P}_1 \cdot \mathbf{z} \tag{24}$$

Figure 4 provides a graphical illustration. This scenario includes as a particular case $\omega_0 = 0$ so that the DC local dissipativity characterization is directly achieved as a function of the parameter ϑ without any extra effort. The high-frequency asymptotic condition $\omega_0 \to \infty$ can be approximated by setting ω_0 to a large value (e.g. two-three orders of magnitude larger than the highest system pole) in (24), or alternatively by splitting differential and algebraic parts in (1) through a canonical decomposition[34,55,56], and repeating the above derivations as restricted to the direct coupling and/or leading asymptotic terms of the transfer function. These details are here omitted; the following derivations and examples assume a finite value or a bounded interval for ω_0.

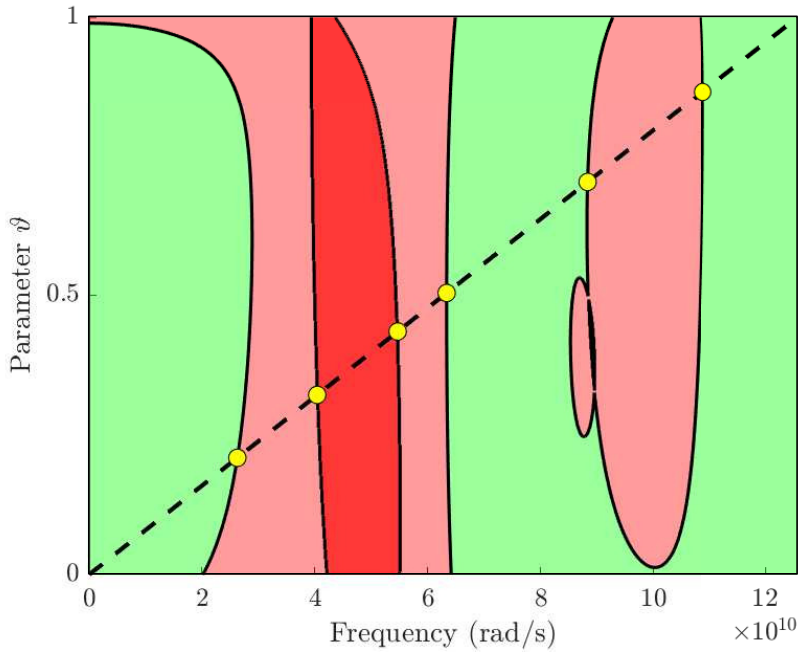

Figure 5 Evaluation of the zero crossings of the boundaries of locally active $\mathcal{A}_i$ and locally dissipative regions D along a generic straight line.

4.1 | Scanning the frequency-parameter plane

The two univariate dissipativity characterizations providing horizontal or vertical cuts of $\mathcal{Z}$ at constant parameter or frequency values are only particular cases. More general strategies can be adopted, as discussed in this section.

Here we consider the intersection of $\mathcal{Z}$ with a generic curve ζ in the plane (ω, ϑ). In particular, we consider the explicit case

$$\omega = f(\vartheta) \tag{25}$$

which combined with (23) leads to the modified problem

$$(\mathbf{P}_0 + \vartheta \mathbf{P}_1 - \mathrm{j} f(\vartheta)\mathbf{J}) \cdot \mathbf{z} = \mathbf{0}. \tag{26}$$

We assume the solutions $(f(\vartheta), \vartheta)$ to (26), to be collected in set $\mathcal{Z}_f \subseteq \mathcal{Z}$, defined as

$$\mathcal{Z}_f := \{(f(\vartheta), \vartheta) : \exists \mathbf{z} \neq \mathbf{0} \text{ solving (26)}\} \tag{27}$$

The representation (26) converts an underdetermined multi-parameter eigenvalue problem into a nonlinear eigenvalue problem[57], whose numerical solution may be challenging in the general case. However, we will show in the following that appropriate choices of $f(\vartheta)$ may indeed lead to quite effective numerical schemes for passivity characterization.

4.1.1 | Linear cuts

Let us assume that the curve (25) is a straight line

$$\omega = f(\vartheta) = \gamma_0 + \gamma_1 \vartheta \tag{28}$$

in which case (26) becomes

$$(\mathbf{P}_0 - \mathrm{j}\mathbf{J}\gamma_0) \cdot \mathbf{z} = -\vartheta\,(\mathbf{P}_1 - \mathrm{j}\gamma_1 \mathbf{J}) \cdot \mathbf{z} \tag{29}$$

representing a standard generalized eigenvalue problem, whose acceptable solutions are for $\vartheta \in \Theta$. The solutions of this eigenproblem provide the intersections of $\mathcal{Z}$ with a generic straight line in the frequency-parameter plane. This can be useful whenever a locally active point $(\mathrm{j}\omega_0, \vartheta_0)$ is known and the extent of the locally active region $\mathcal{A}$ including this point along a given direction is desired. This case is illustrated in Fig. 5.

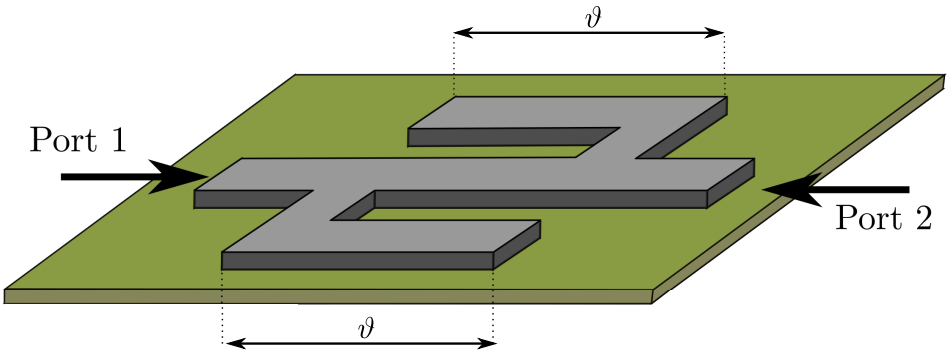

Figure 6 View of a double-folded microstrip filter parameterized by the length of two stubs.

4.1.2 | Polynomial cuts

A direct generalization of the above linear cut is obtained through a degree-D polynomial curve

$$f(\vartheta) = \gamma_0 + \gamma_1 \vartheta + \cdots + \gamma_D \vartheta^D \tag{30}$$

leading to

$$\left[\mathbf{P}_0 - \mathrm{j}\mathbf{J}\gamma_0 + (\mathbf{P}_1 - \mathrm{j}\gamma_1\mathbf{J})\vartheta - \mathrm{j}\mathbf{J}(\gamma_2\vartheta^2 + \cdots + \gamma_D\vartheta^D)\right] \cdot \mathbf{z} = \mathbf{0} \tag{31}$$

which is recognized as a Polynomial Eigenvalue Problem (PEP)[58], for which reliable numerical solvers are available.

The interest in such polynomial formulation lies in the possibility of choosing polynomial functions that, upon degree elevation, scaling, and shifting operations may be designed to scan uniformly a given region of the frequency-parameter plane. Examples are Chebychev polynomials, whose effectiveness is demonstrated in next section through several numerical examples.

5 | NUMERICAL EXPERIMENTS

This section is organized in two parts. First, we test various strategies for performing one-dimensional cuts in the frequency-parameter plane, with the objective of assessing the performance of proposed constrained multi-parameter eigenvalue formulation in the identification of boundaries between locally active and dissipative regions. Then, we propose and test a simple algorithm aimed at finding all locally active regions of a LTI model, by scanning the entire frequency-parameter plane.

5.1 | Testing different polynomial degrees

Here we test the proposed method with increasingly complex polynomial representations of the curve f in (25). Starting with a simple constant, we increase complexity up to a polynomial order $D = 4$. All experiments are based on first-kind Chebychev polynomials, due to their distinctive "oscillatory" behavior that makes them particularly suited to cover a predefined compact domain.

The running example is a lumped model of a 2-port planar microwave structure, namely the double-folded microstrip filter originally presented in[59,60] and depicted in Fig. 6. The filter response is parameterized by the length of the two stubs $\vartheta \in [2.08, 2.28]$ mm. Following the data-driven model reduction algorithm presented in[7,61], a parameterized model was generated starting from sampled frequency responses obtained from a full-wave electromagnetic solver up to $\omega_{max} = 20$ GHz. The

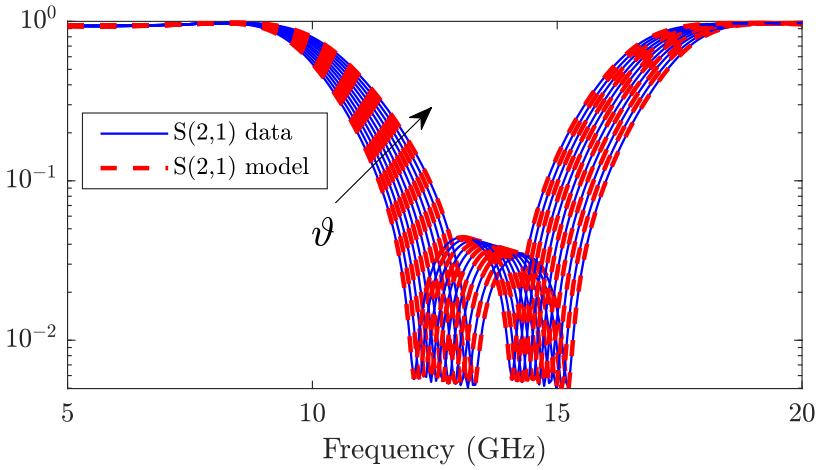

Figure 7 Parameterized transmission coefficient of a double-folded microstrip filter. Solid blue-lines: raw data; red-dashed lines: parameterized model responses.

description realization of the model (1) is parameterized by Chebychev polynomials of degree 2 and has size $N = 32$. For illustration, Fig. 7 depicts the parameterized transmission coefficient of the filter, comparing reduced-order model responses to the corresponding original field solver data.

5.1.1 | D = 0

In case of constant parameterization $\omega = f(\vartheta) = \gamma_0$, the presented procedure fills the solution set $\mathcal{Z}_f$ for a predefined and fixed frequency value $\gamma_0 = \bar{\omega}$, i.e.,

$$\mathcal{Z}_f = \{(\bar{\omega}, \vartheta_1), (\bar{\omega}, \vartheta_2), \dots\} \tag{32}$$

Figure 4 shows the results of the proposed approach for $\bar{\omega} = 10$ GHz, confirming that the solutions $\vartheta_1, \vartheta_2, \dots$ are placed exactly at the intersections (yellow dots) of the straight line $\omega = \bar{\omega}$ with the set $\mathcal{Z}$. The time required to find this solution using a standard laptop was about 0.01 seconds.

5.1.2 | D = 2

In this second case, we consider the quadratic Chebychev polynomial $f(\vartheta) = 2\vartheta^2 - 1$. In order to match the frequency and parameter scales, we introduce the following renormalization

$$\omega = \Delta^+ + f(\vartheta)\Delta^- \tag{33}$$

with $\Delta^+ = (\omega_{\max} + \omega_{\min})/2$, $\Delta^- = (\omega_{\max} - \omega_{\min})/2$, that maps the $[-1,\ 1]$ subdomain of $f(\vartheta)$ into $[\vartheta_{\min}, \vartheta_{\max}]$, and the corresponding $[-1,\ 1]$ image in $[\omega_{\min},\ \omega_{\max}]$. For illustration, we set $\omega_{\min} = 0$ and $\omega_{\max} = 20$ GHz.

The results of this second test required about 0.046 seconds and are depicted in Figure 8. As expected, the solutions in set $\mathcal{Z}_f$ are placed along a parabola described by a the second-order Chebychev polynomial.

5.1.3 | D = 4

In this latter case, we use a fourth order Chebychev polynomial leading to the representation

$$\omega = \Delta^+ + (8\vartheta^4 - 8\vartheta^2 + 1)\Delta^- \tag{34}$$

whose results are depicted in Fig. 9. Also in this case all computed eigenvalues track the transition between locally active and dissipative regions along the considered trajectory. Total runtime was about 0.23 seconds.

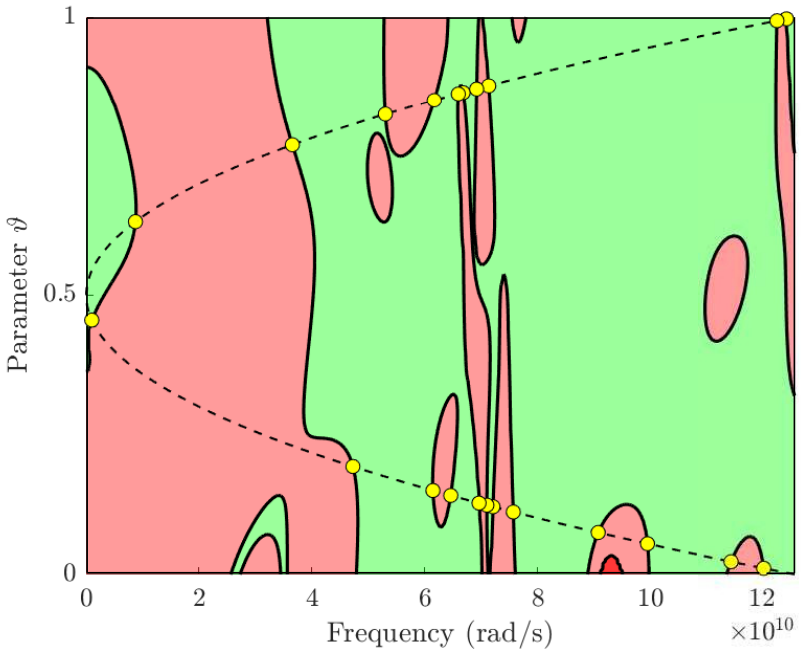

Figure 8 Evaluating the transitions between locally active and locally dissipative regions along a curve defined through a second-order Chebychev polynomial.

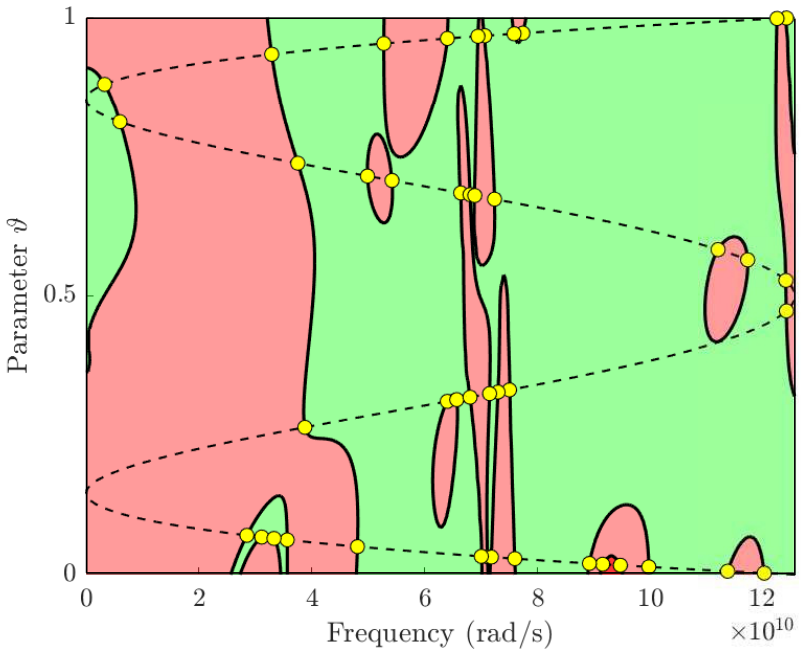

Figure 9 As in Fig. 8, but along a curve defined through a fourth-order Chebychev polynomial.

5.1.4 | Discussion

These results confirm that the higher the polynomial degree, the higher is the resolution of the sampling, since more intersections are concurrently found by the eigenvalue solver. At the same time, the computation of these solutions becomes slower due to the increased order of the associated polynomial eigenvalue problem. Therefore, in order to uniformly scan the frequency-parameter plane, a compromise is required to keep computing time within reasonable limits.

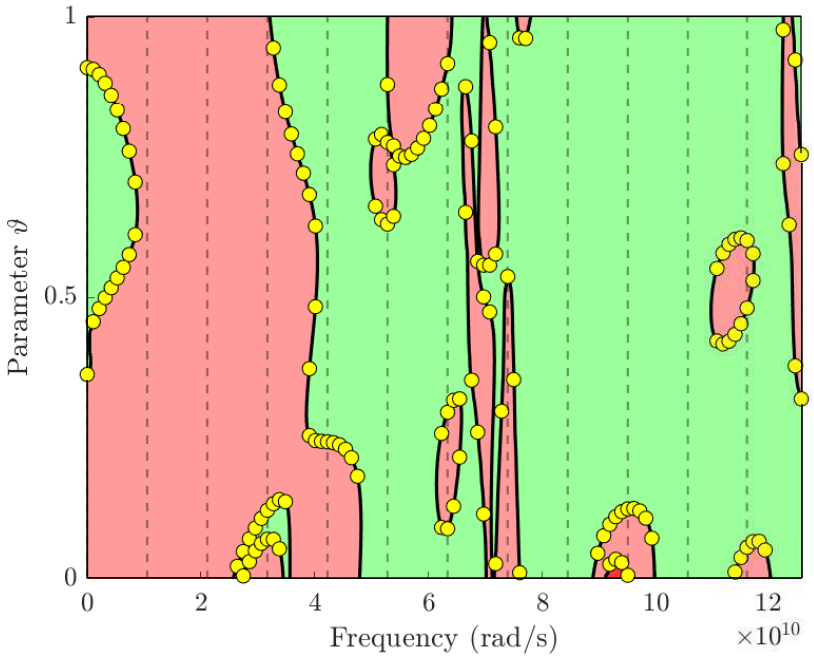

Figure 10 Passivity check performed with shifted vertical cuts.

5.2 | A dissipativity check algorithm

A convenient approach for setting up an algorithm for checking uniform dissipativity is to repeatedly compute the solution of (31) through low-order and iteratively shifted polynomial trajectories. This approach is able to break the dependence between the sampling resolution and the associated computational complexity, which scales unfavorably with the polynomial degree D. We thus set up an iterative scheme that, at each iteration $\kappa = 1, \dots, K$, solves the modified PEP (31) based on a shifted trajectory

$$\omega_\kappa = f(\vartheta - \vartheta^s_\kappa) \tag{35}$$

where the shifts ϑ^s_κ change at each iteration. Several strategies can be devised for adapting the shifts through iterations, including hierarchical and adaptive schemes. In the following tests, we document a simple uniform shifting strategy where the shifts ϑ^s_κ linearly span the range $[\vartheta_{\min}, \vartheta_{\max}]$, and we will use a fixed number of iterations $K = 100$. The three polynomial cases of degree $D = 0, 2, 4$ are discussed.

5.2.1 | D = 0

In case of constant shifted parameterization, we just set

$$\omega_\kappa = \gamma_{0,\kappa}, \tag{36}$$

without the need of employing the more general form (35). The terms $\gamma_{0,\kappa}$ are defined a-priori in order to linearly span the considered band of interest $[\omega_{\min}, \omega_{\max}]$. The results of this test are illustrated in Figure 10, where only a subset of the shifts $\gamma_{0,\kappa}$ is depicted through dashed vertical lines, in order to maintain readability of the plot. The yellow dots represent the union of all computed eigenvalues. We see that the set $\mathcal{Z}$ collecting the boundaries between $\mathcal{A}_1$, $\mathcal{A}_2$ and $\mathcal{D}$ is resolved with a good density of points. The total CPU time required to obtain these results is 0.7 seconds.

5.2.2 | D = 2

The resolution can be increased by using shifted quadratic trajectories

$$\omega_\kappa = \Delta^+ + (2(\vartheta - \vartheta^s_\kappa)^2 - 1)\Delta^- \tag{37}$$

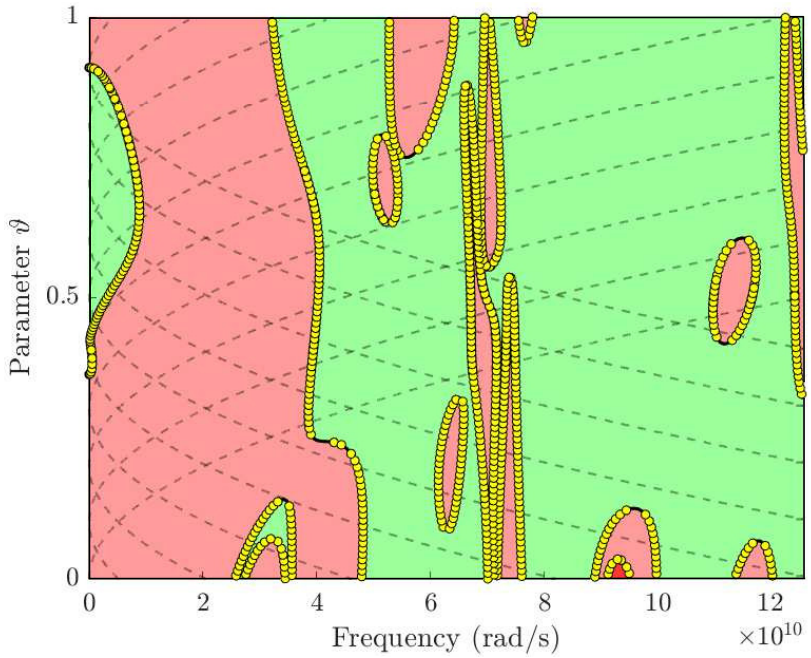

Figure 11 Passivity check performed with shifted curves defined by second order Chebychev polynomials.

As demonstrated in Figure 11, the density of the points along the set $\mathcal{Z}$ has significantly increased with respect to the constant case $D = 0$, leading to a quite accurate tracking of the boundaries. Also in this plot only a subset of quadratic trajectories is depicted with dashed lines. The total CPU time to obtain these results is about 5.1 seconds.

5.2.3 | D = 4

We conclude our tests with fourth-order Chebychev polynomial trajectories

$$\omega = \Delta^+ + (8(\vartheta - \vartheta_\kappa^s)^4 - 8(\vartheta - \vartheta_\kappa^s)^2 + 1)\Delta^- \tag{38}$$

whose results are depicted in Figure 12. The overall CPU time required to compute these solutions is about 31 seconds. The increased computational effort (approximately 6× larger if compared with the case $D = 2$) is not justified, since it does not provide an increased resolution, at least for this test case.

5.3 | An integrated inductor

In this section, we demonstrate the usefulness of the proposed dissipativity check algorithm on an application test case. We consider the model of an integrated inductor for automotive radar applications. The inductor has a square footprint, whose conductive traces are parameterized by their width, varying in the range $[2000,\ 5500]\ \mu m$. The electrical behavior of the inductor is known from 11 parametric scattering responses linearly covering the $[2000,\ 5500]\ \mu m$ range and spanning the band $[0,\ 300]$ GHz, evaluated by a full-wave field solver. A stable parameterized LTI model of the form (1) has been constructed with $N = 75$ states and polynomial order $\bar{\ell} = 2$. Figure 13 demonstrates the model accuracy by comparing the raw data (blue solid lines) with the associated model responses (red-dashed lines).

This initial model was not passive, as confirmed by the top-left panel of Figure 14 where the proposed passivity characterization results are depicted. The model was then processed by a passivity enforcement scheme[29], which iteratively perturbs the model coefficients by formulating local passivity constraints. The formulation of these constraints is based on the information about the regions $\mathcal{A}_i$ provided by the proposed characterization. Figure 14 shows that the red violation areas are progressively eliminated through iterations, until the model is uniformly passive as highlighted in the bottom-right panel of Figure 14. As a conclusion, this uniformly passive model can be safely used in a CAD environment as a parameterized library component model, in particular in any transient simulation required as part of design centering, optimization, sensitivity or Monte Carlo analyses.

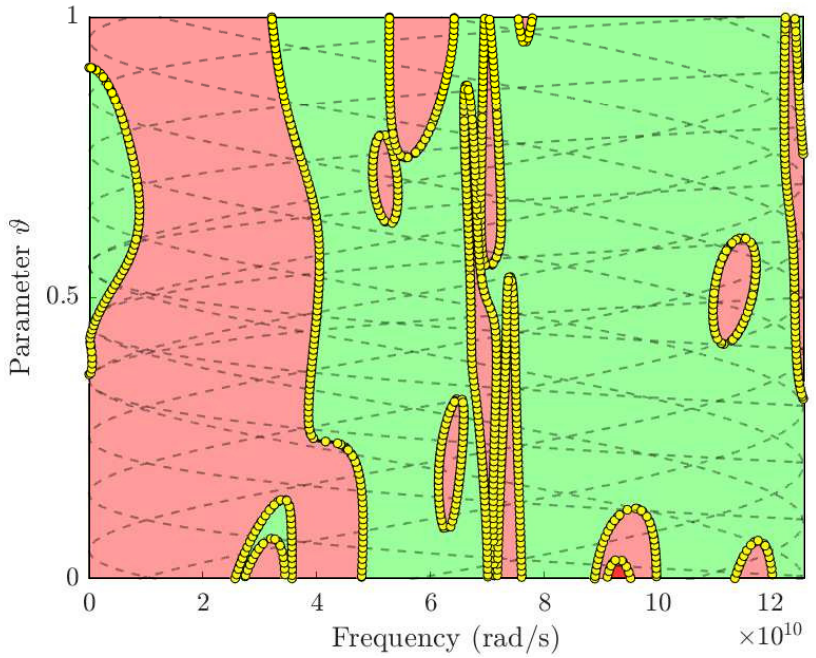

Figure 12 Passivity check performed with shifted curves defined by fourth order Chebychev polynomials.

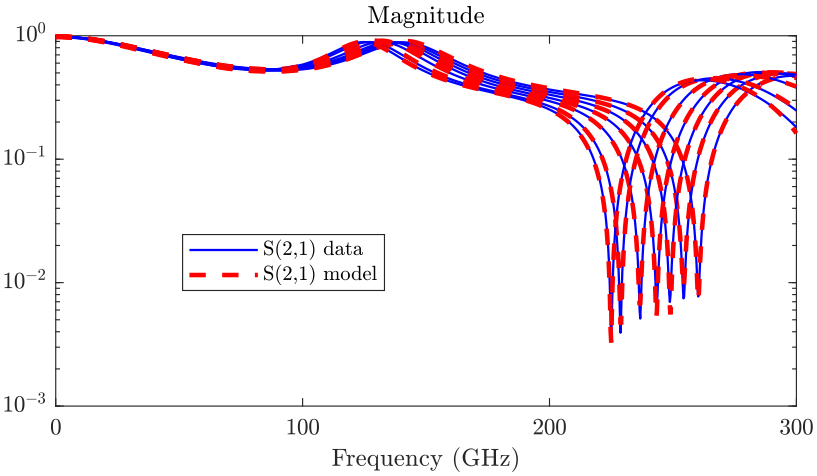

Figure 13 Comparing raw data (blue solid lines) with the associated parameterized LTI scattering model responses (red dashed lines).

5.4 | A network with coupled microstrip lines

We now consider a more complex distributed electrical structure, namely the 7-port coupled microstrip transmission line network depicted in Fig. 15, adapted from[62]. This structure includes three pairs of lossy coupled microstrip lines, placed over a lossy substrate with nominal $\epsilon_r = 3.7$ and $\tan\delta = 0.02$. The coupled line pairs have a common height $h = 10\ \mu m$ and separation $d = 40\ \mu m$. The nominal length for the input coupled lines W1-W2 is $l_{1,2} = 1\ mm$, whereas $l_{3,4} = l_{5,6} = 30\ mm$ for the other pairs W3-W4 and W5-W6. In our tests, we consider both material and geometry-induced variability. In particular, we consider as free parameters the relative dielectric constant ϵ_r and the length of line pairs W3-W4 and W5-W6. These parameters are allowed to vary within prescribed ranges, defined as $[\underline{\epsilon}_r, \bar{\epsilon}_r]$ for ϵ_r and $[\underline{l}_{3,4}, \bar{l}_{3,4}]$, $[\underline{l}_{5,6}, \bar{l}_{5,6}]$ for the lines, respectively, where the ranges are defined as a 10% variation around the respective nominal values.

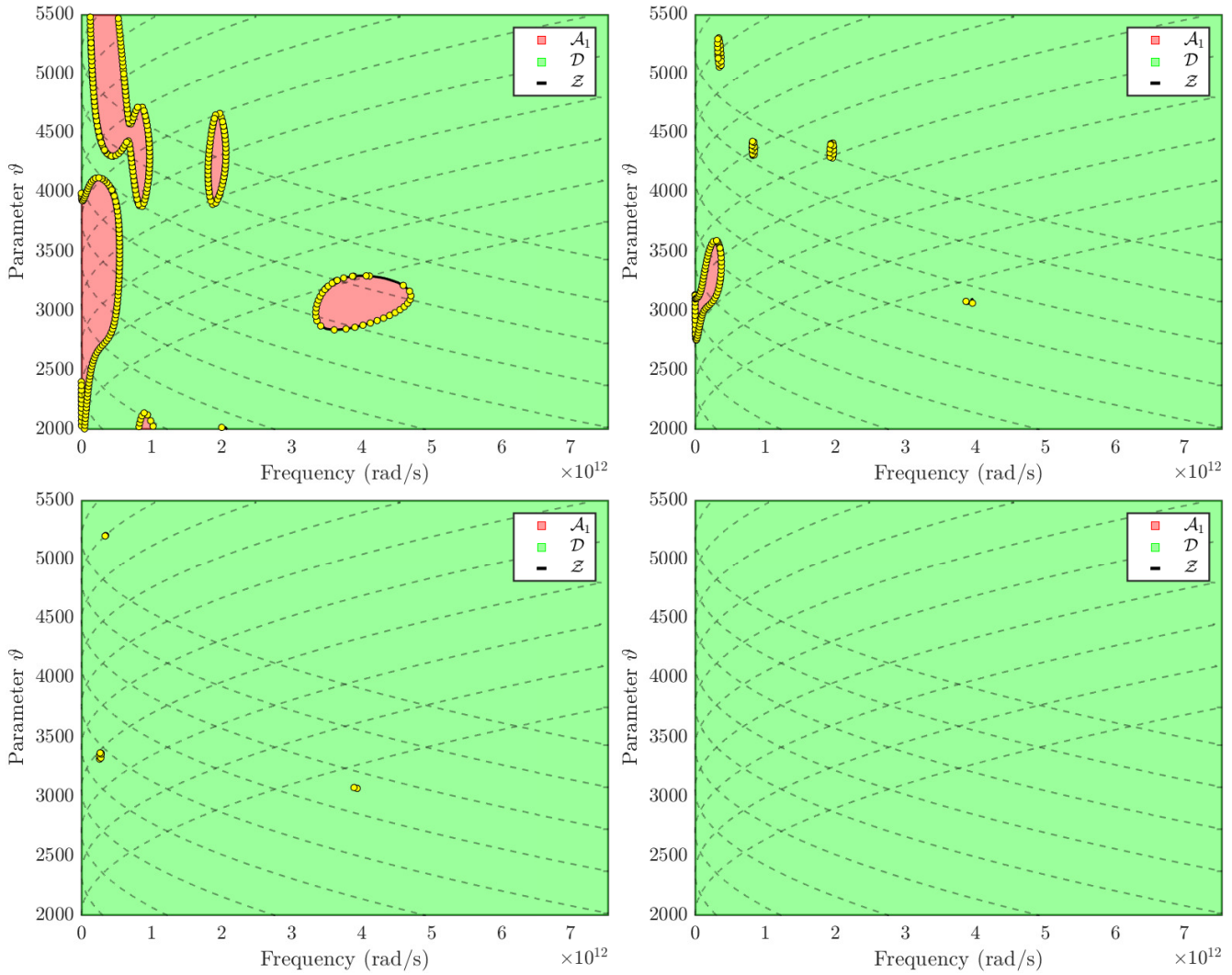

Figure 14 Evolution of passivity violation regions detected with the proposed approach. From the top to bottom: initially non-passive model, intermediate enforcement iterations, final passive model.

First, in order to assess the capabilities of the adopted *Chebychev* polynomial bases in representing the variability of the system responses, we consider three different parameterizations:

- *Parameterization 1*: The free parameter is ε_r, whereas the line lengths are fixed as $l_{3,4} = \underline{l}_{3,4}$, $l_{5,6} = \underline{l}_{5,6}$;
- *Parameterization 2*: The free parameter is ε_r, whereas the line lengths are fixed as $l_{3,4} = \bar{l}_{3,4}$, $l_{5,6} = \bar{l}_{5,6}$;
- *Parameterization 3*: The free parameter are the lengths $l_{3,4} = l_{5,6}$, whereas ε_r is fixed to $\underline{\varepsilon}_r$.

For each of these cases, we start with a reference training dataset (obtained with repeated HSPICE runs) composed of $K = 801$ scattering frequency samples over a 20 GHz bandwidth, evaluated over 50 linearly spaced parameter values within the corresponding range. Based on these data, we build three parameterized models through the well-established *Parameterized Sanathanan-Koerner iteration*[7,63], by tuning number of poles and parameterization order such that the RMS absolute model-data error is less than 1%. The three resulting models have the following characteristics, with reference to the realization (1)

- *Model 1*: number of states $N = 259$, parameterization order $\bar{\ell} = 3$, model-data error $3.37 \cdot 10^{-3}$;
- *Model 2*: number of states $N = 259$, parameterization order $\bar{\ell} = 3$, model-data error $8.09 \cdot 10^{-3}$;
- *Model 3*: number of states $N = 259$, and parameterization order $\bar{\ell} = 5$, model-data error $8.62 \cdot 10^{-3}$.

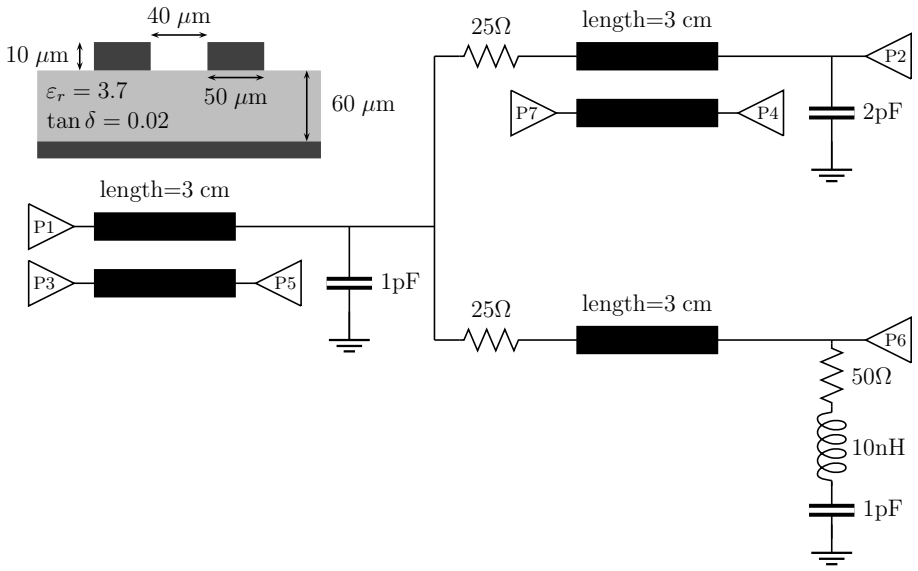

Figure 15 A distributed electrical network, adapted from[62]

The panels of Figure 16 provide a visual accuracy test for the three models on the representative scattering matrix element (5, 4), for some randomly chosen validation samples.

Based on these numerical results, we can conclude that the selected Chebychev polynomial bases are capable of approximating the parametric behavior of both geometrical and material characteristics. In addition, in order to prove the capabilities of the proposed approach, we apply our passivity verification strategy to the *model 3* of Section 5.4, which embeds the largest parametric responses variability. Using a quadratic ($D = 2$) Chebychev polynomial parameterization, we obtain the results shown in Figure 17. The figures depict the frequency-parameter plane scanned with the proposed sampling procedure, performed with 100 linearly spaced shifts ϑ_κ^s. The figures confirm that all the boundaries of all the passivity violations have been detected and tracked. We remark that this structure leads to $P = 7$ independent singular value trajectories, each potentially leading to a set of curves separating locally dissipative from locally active regions, and whose union forms the set $\mathcal{Z}$. For ease of visualization, we report only the reference set $\mathcal{Z}_0$, denoting the interface of active ($\mathcal{A}$) and dissipative ($\mathcal{D}$) regions.

5.5 | On the computational complexity

In this Section, we provide a detailed analysis on the computational complexity of the proposed passivity verification method. As a reference structure, we consider again the microstrip network of Section 5.4, for which the relative dielectric constant is set to the nominal value $\varepsilon_r = 3.7$, while the line lengths $l_{3,4} = l_{5,6}$ vary in their respective 10% ranges.

In the following, we will consider the time required for a single solution of the PEP (31), based on a reference second-order Chebychev polynomial parameterization. In order to investigate the runtime dependence on each individual size/order, we sweep independently the following variables:

- number of ports P,
- number of states N,
- polynomial order $\bar{\ell}$,
- PEP parameterization order D.

We remark that

1. the PEP matrices $\mathbf{P}_0$, $\mathbf{P}_1$ and $\mathbf{J}$ are square with size $2\bar{\ell}(N + P)$;

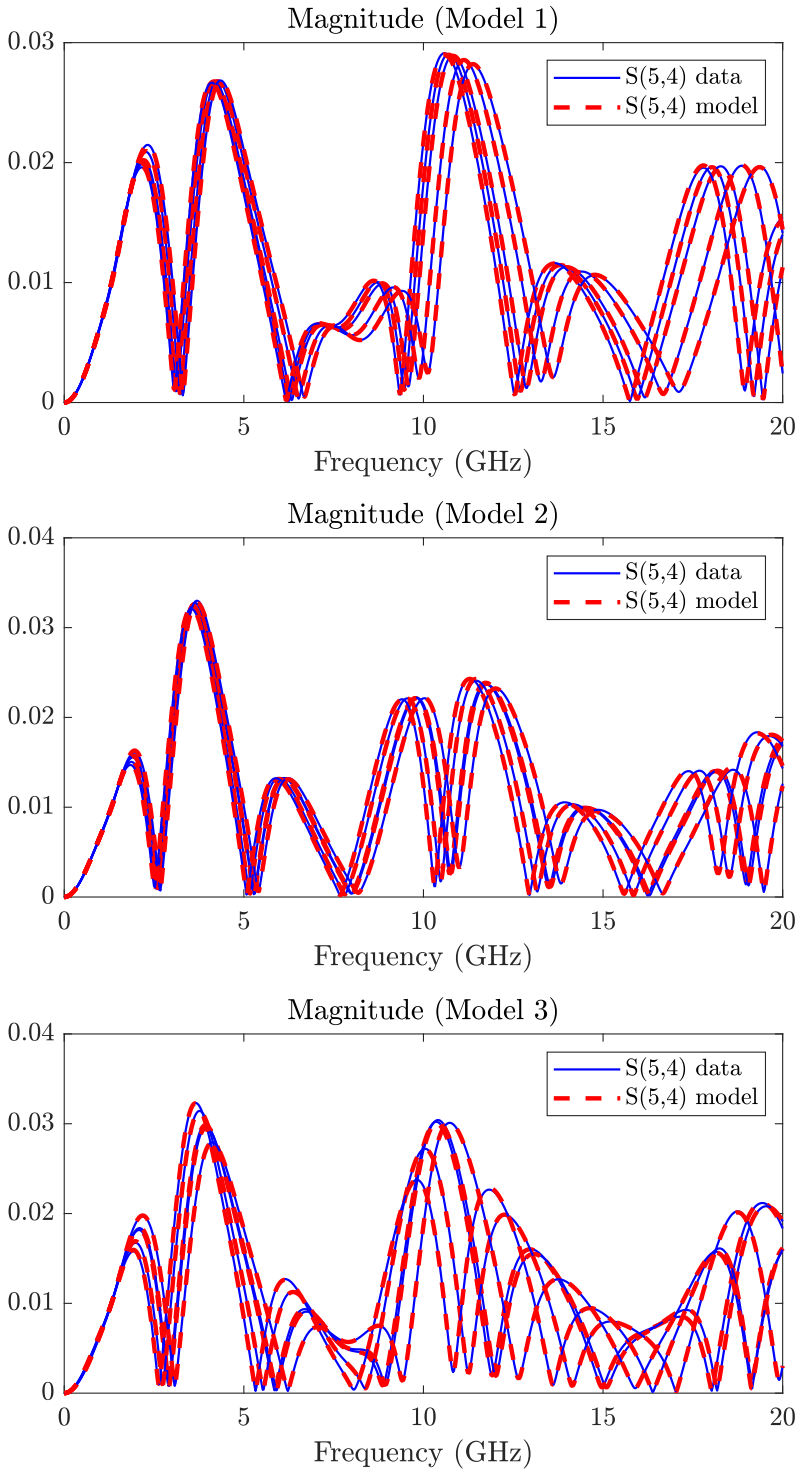

Figure 16 Visual accuracy comparison of the models 1,2 and 3 on a representative scattering matrix element. Top panel: model 1; middle panel: model 2; bottom panel: model 3.

2. the complexity of the eigenvalue extraction scales theoretically as $O(n^3)$.

We therefore expect the PEP computational complexity to scale with the third power of P, N and $\bar{\ell}$.

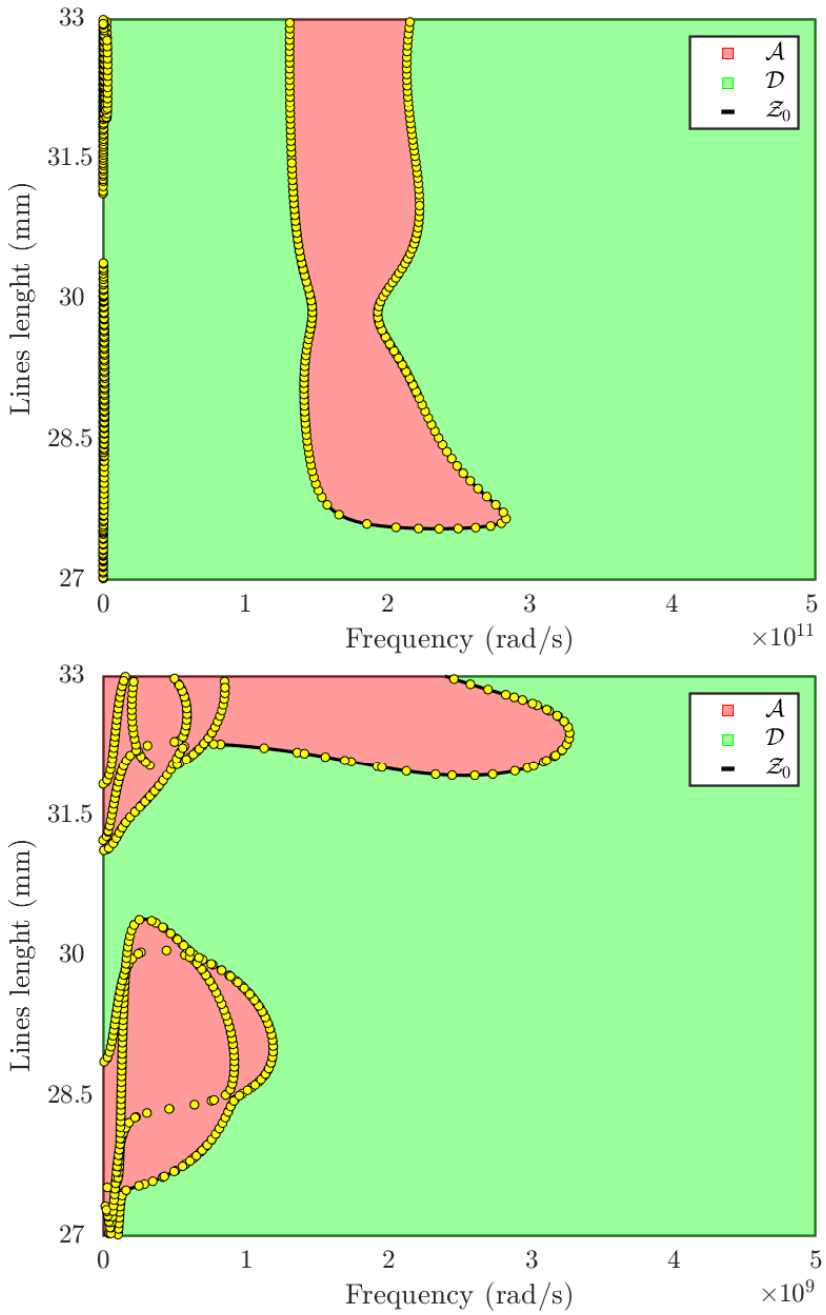

Figure 17 Results of the proposed passivity check method on the coupled transmission line model. Top and bottom panels provide two different views of the same results by zooming on different frequency bands. In both panels, only the separation line $\mathcal{Z}_0 \subseteq \mathcal{Z}$ between the active ($\mathcal{A}$) and dissipative ($\mathcal{D}$) regions is shown. The yellow dots evaluated with the proposed method that are placed inside the active regions denote points where the number of negative eigenvalues $\lambda(\mathrm{j}\omega, \vartheta)$ of $\mathbf{\Psi}(\mathrm{j}\omega, \vartheta)$ becomes larger than one.

In addition, it is known[58] that the solution of a PEP of order D (through linearization, as implemented in MATLAB) involving a generic $M \times M$ matrix $\mathbf{X}$, demands for the eigenvalue extraction of a $M(D+1)$-sized square matrix. Being all the other variables fixed, we therefore expect the complexity of the PEP to scale as $O(D^3)$. We will check the above theoretical results on our numerical tests.

5.5.1 | Number of ports

The dependence on the number of ports P is assessed by processing a set of $P \times P$ submodels obtained by terminating the ports $P+1, P+2, \ldots$ into the reference port resistance defining the scattering system (50Ω). For each of these models, we solve (only once) the associated PEP. The results are shown in the top-left panel of Figure 18.

5.5.2 | Number of states

In order to provide a meaningful comparison, we consider 4 partitions of the original dataset, defined by a increasingly large frequency bands (namely 5, 10, 15 and 20 GHz). Setting a target accuracy of 1%, the corresponding models need an increasingly large number of poles (thus states) to fully capture the dynamic behavior, due to the distributed transmission-line segments in the network. From our numerical experiments, the accuracy constraint is reached using 10, 20, 30 and 40 poles, with a corresponding number of states equal to 70, 140, 210 and 280. The runtime results applied to these four models are depicted in the top-right panel of Figure 18.

5.5.3 | Polynomial order $\bar{\ell}$

As in the previous case, to make the comparison meaningful, we reduce the extent of the parameter space by leaving unchanged the target accuracy threshold (1%). A smaller parameter range induces less variability and requires correspondingly a lower order $\bar{\ell}$ in the model parameterization. We consider four different cases with $\bar{\ell}$ equal to 2, 3, 4 and 5, respectively.

The PEP runtime results are shown in the bottom-left panel of Figure 18. We observe a mismatch between our theoretical prediction and the numerical experiments, with an experimentally determined complexity approximately $O(\bar{\ell}^2)$ (red-dashed line), instead of $O(\bar{\ell}^3)$ (black-dashed line). Although we do not have a clear explanation, we believe that this (beneficial) improvement is due to the particular structure (block and sparse) of the PEP matrices, for which the adopted MATLAB solver is likely able to compute the eigenvalues more efficiently.

5.5.4 | PEP order D

Finally, we compare the runtime for increasingly large order for the PEP parameterization. Here, we consider a model representing the complete broadband parametric dataset, synthesized with $N = 259$ states and $\bar{\ell} = 5$. The numerical results for PEP parameterizations D ranging from 2 to 8 are shown in the bottom-right panel of Figure 18.

5.6 | Comparison with existing techniques

Prior to this work, the Authors worked extensively on the problem of parametric passivity verification and enforcement [29,30,48]. For completeness, we compare the results obtained with the presented approach with previous works, in particular with the adaptive sampling strategy presented in [30], where the Authors presented a complete framework for the passivity verification and enforcement based on iterated post-processing model perturbations. The main enabling factor for the enforcement procedure is an efficient hierarchical subdivision of the parameter space (based on repeated evaluation of constant-parameter Hamiltonian or SHH eigenvalues) aimed at detecting a reduced set of frequency-parameter combinations where to formulate convex passivity constraints.

Although both the presented algorithm and the one devised in [30] sample the frequency-parameter space to characterize the dissipativity characteristics, they serve two different purposes:

- the proposed approach aims at finely resolving the boundaries of the locally active and locally dissipative regions, while
- the strategy [30] attempts the derivation of a minimal set of frequency-parameter combinations where to formulate passivity constraints.

Figure 19 depicts the results of the adaptive sampling [30] applied to the same filter testcase of Fig. 6. All the relevant passivity violations are detected with a sufficient resolution to formulate effective passivity constraints. However, the obtained resolution is modest compared with the proposed strategy (see Figure 12 obtained with 100 fourth-order polynomial shifts; note that only the yellow dots are returned by the sampling algorithms and that the color shades are reported only for visualization of the reference model behavior and are not used by the algorithms). This consideration has a direct implication on the computational runtime, that is approximately 3× slower for the proposed approach due to the much increased resolution.

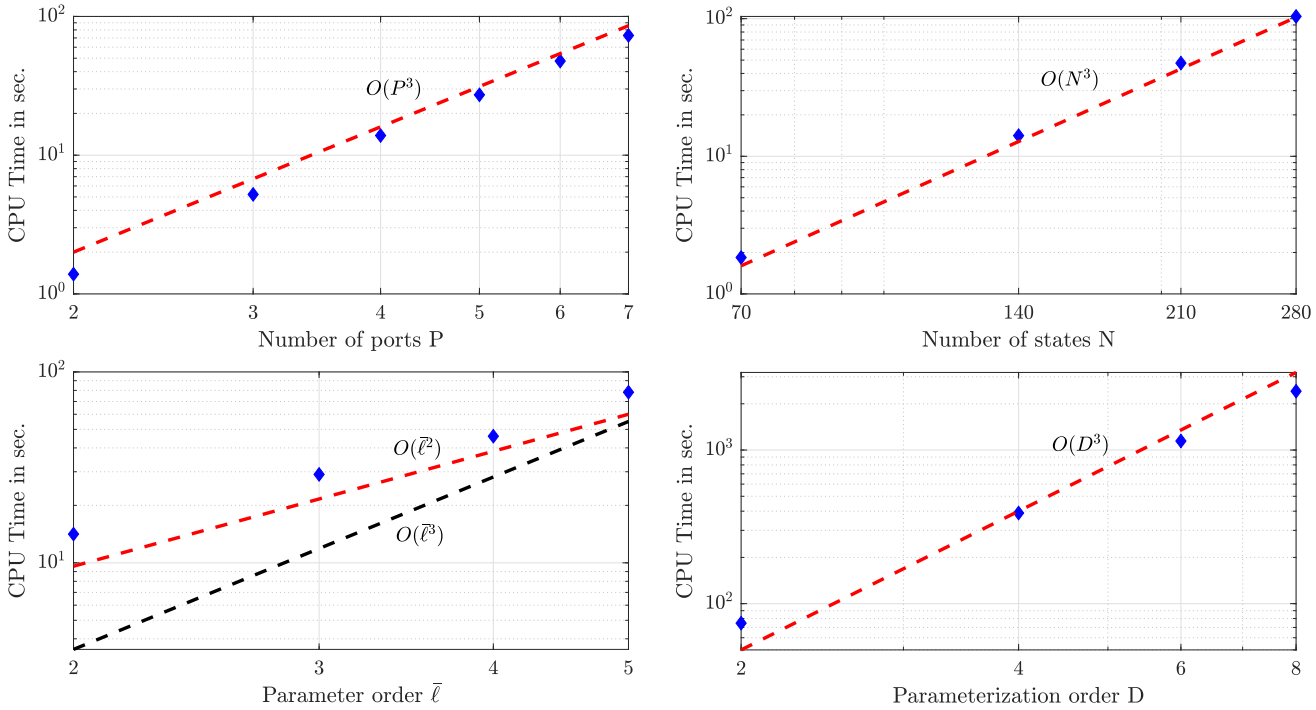

Figure 18 Runtime required for the PEP solution. The markers depict the computed runtimes, while the dashed lines represent reference polynomial scaling laws. Top-left panel: number of ports P. Top-right panel: number of states N. Bottom-left panel: parameter order $\bar{\ell}$. Bottom-right panel: PEP parameterization order D.

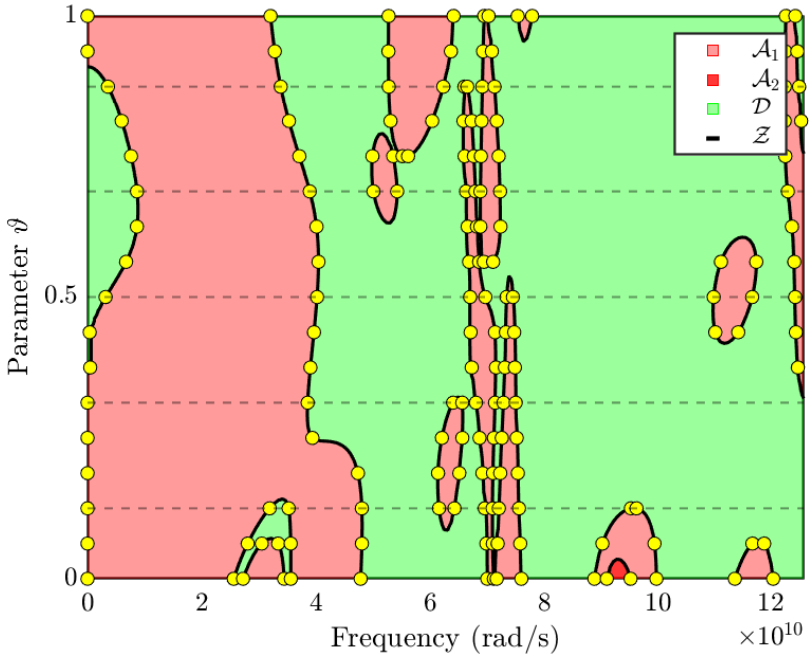

Figure 19 As in Figure 12, but obtained running the hierarchical adaptive sampling presented in [30].

In order to ease a performance comparison between these two approaches, a second test was performed by executing the two schemes approximately with the same runtime. This condition was simply achieved by reducing the number of polynomial shifts of proposed approach to 33, i.e. approximately $1/3$ of the original 100. The results of this experiment are shown in

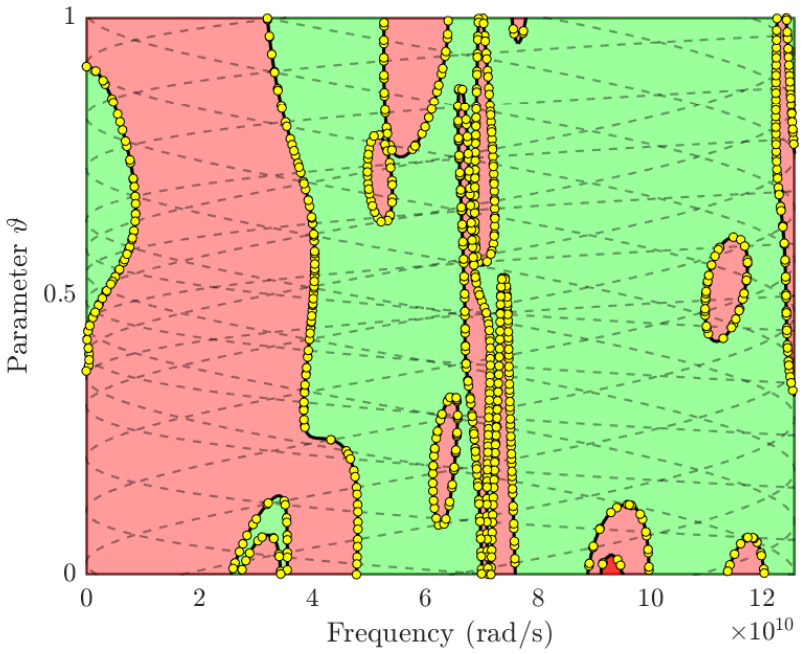

Figure 20 As in Figure 12, but obtained running proposed scheme with 33 fourth-order polynomial shifts instead of 100.

Figure 20, which confirms that even with the same computing requirements the proposed approach allows for a significantly better resolution with respect to[30].

6 | CONCLUSIONS

This paper presented a novel characterization of the dissipativity of lumped parameterized reduced-order models of linear time-invariant circuits and systems. The characterization is derived from well-known spectral representations based on Hamiltonian eigenvalues, through an extension to the parameterized case. The resulting dissipativity test requires the solution of an underdetermined multi-parameter eigenvalue problem, which is obtained numerically by constraining the solution to a set of one-dimensional polynomial trajectories in the frequency-parameter plane.

The results show that the iterative application of proposed test based on low-order shifted polynomial trajectories results particularly effective in tracking the boundaries of locally dissipative and locally active regions, thus enabling integration with existing passivity enforcement methods based on local perturbations.

The main limitation of proposed approach is its restriction to a single parameter. Practical design application scenarios involve possibly several independent parameters, and a comprehensive dissipativity test and classification algorithm in such high-dimensional setting still appears unfeasible. Future research efforts in this direction will be devoted to softening the one-dimensional requirement, with the objective of understanding the feasibility of higher dimensional characterizations.

□

APPENDIX

A PROOF OF THEOREM 1

This section provides the derivation of the matrices $\mathbf{P}_0$, $\mathbf{P}_1$, $\mathbf{J}$ in (23), thus providing a constructive proof of Theorem 1.

We start by re-writing the definitions (3) of parameterized matrices $\mathbf{A}(\vartheta)$ and $\mathbf{C}(\vartheta)$ by highlighting the highest degree terms, as

$$\begin{aligned}\mathbf{A}(\vartheta) &= \sum_{\ell=0}^{\bar{\ell}-1} \mathbf{A}_\ell \xi_\ell(\vartheta) + \mathbf{A}_{\bar{\ell}} \xi_{\bar{\ell}}(\vartheta) \\ \mathbf{C}(\vartheta) &= \sum_{\ell=0}^{\bar{\ell}-1} \mathbf{C}_\ell \xi_\ell(\vartheta) + \mathbf{C}_{\bar{\ell}} \xi_{\bar{\ell}}(\vartheta)\end{aligned} \tag{A1}$$

Inserting in (19) leads to

$$\begin{cases} \mathrm{j}\omega_0 \mathbf{E}\mathbf{r}_0 = \sum_{\ell=0}^{\bar{\ell}-1} \mathbf{A}_\ell \mathbf{r}_\ell + \mathbf{A}_{\bar{\ell}} \mathbf{r}_{\bar{\ell}} + \mathbf{B}\mathbf{v}_0 \\ \mathrm{j}\omega_0 \mathbf{E}^\mathsf{T} \mathbf{q}_0 = -\sum_{\ell=0}^{\bar{\ell}-1} \mathbf{C}_\ell^\mathsf{T} \mathbf{w}_\ell - \mathbf{C}_{\bar{\ell}}^\mathsf{T} \mathbf{w}_{\bar{\ell}} - \sum_{\ell=0}^{\bar{\ell}-1} \mathbf{A}_\ell^\mathsf{T} \mathbf{q}_\ell - \mathbf{A}_{\bar{\ell}}^\mathsf{T} \mathbf{q}_{\bar{\ell}} + \\ \qquad\qquad - \sum_{\ell=0}^{\bar{\ell}-1} \mathbf{C}_\ell^\mathsf{T} \mathbf{S}^\mathsf{T} \mathbf{v}_\ell - \mathbf{C}_{\bar{\ell}}^\mathsf{T} \mathbf{S}^\mathsf{T} \mathbf{v}_{\bar{\ell}} \\ \mathbf{w}_0 - \sum_{\ell=0}^{\bar{\ell}-1} \mathbf{R}\mathbf{C}_\ell \mathbf{r}_\ell - \mathbf{R}\mathbf{C}_{\bar{\ell}} \mathbf{r}_{\bar{\ell}} = \mathbf{0} \\ \sum_{\ell=0}^{\bar{\ell}-1} \mathbf{S}\mathbf{C}_\ell \mathbf{r}_\ell - \mathbf{S}\mathbf{C}_{\bar{\ell}} \mathbf{r}_{\bar{\ell}} + \mathbf{B}^\mathsf{T} \mathbf{q}_0 + \mathbf{Q}\mathbf{v}_0 = \mathbf{0} \end{cases} \tag{A2}$$

where we defined $\mathbf{r}_\ell = \mathbf{r}_\ell(\vartheta) = \mathbf{r}\, \xi_\ell(\vartheta)$ and similarly for vectors $\mathbf{q}_\ell$, $\mathbf{v}_\ell$ and $\mathbf{w}_\ell$. This system includes $2\bar{\ell}(N+P)$ unknowns and $2(N+P)$ equations only. However, we can add a total of $2(\bar{\ell}-1)(N+P)$ equations using the recurrence relations of vectors $\mathbf{r}_\ell$, $\mathbf{q}_\ell$, $\mathbf{v}_\ell$ and $\mathbf{w}_\ell$, which are inherited from (4). In particular, we have

$$\begin{cases} \mathbf{r}_1 - \alpha_0 \vartheta \mathbf{r}_0 = 0 \\ \mathbf{r}_2 - \alpha_1 \vartheta \mathbf{r}_1 - \beta_1 \mathbf{r}_1 = 0 \\ \mathbf{r}_3 - \alpha_2 \vartheta \mathbf{r}_2 - \beta_2 \mathbf{r}_2 - \delta_2 \mathbf{r}_1 = 0 \\ \vdots \\ \mathbf{r}_{\bar{\ell}-1} - \alpha_{\bar{\ell}-2} \vartheta \mathbf{r}_{\bar{\ell}-2} - \beta_{\bar{\ell}-2} \mathbf{r}_{\bar{\ell}-2} - \delta_{\bar{\ell}-2} \mathbf{r}_{\bar{\ell}-3} = 0 \end{cases} \tag{A3}$$

and similarly for $\mathbf{q}_\ell$, $\mathbf{v}_\ell$ and $\mathbf{w}_\ell$. The latter relations, together with (A2), form a square linear system with size $2\bar{\ell}(N+P)$ in the unknowns $\mathbf{r}_\ell$, $\mathbf{q}_\ell$, $\mathbf{v}_\ell$, $\mathbf{w}_\ell$, with $\ell = 0, \dots, \bar{\ell}-1$. This system is linearly parameterized by ω_0 and ϑ.

Our goal is now to write systems (A2) and (A3) in a concise matrix form. To this end, let us introduce the following matrices

$$\mathbf{K}_{\mathbf{Z}}^{(d_1,d_2)} = \begin{pmatrix} \mathbf{Z} & \mathbf{0}_{d_1,d_2(\bar{\ell}-1)} \\ \mathbf{0}_{d_1(\bar{\ell}-1),d_2} & \mathbf{0}_{d_1(\bar{\ell}-1),d_2(\bar{\ell}-1)} \end{pmatrix}, \qquad \mathbf{T}_{\mathbf{Z}} = [\mathbf{Z}_0, \dots, \mathbf{Z}_{\bar{\ell}-3}, \widehat{\mathbf{Z}}_{\bar{\ell}-2}, \widehat{\mathbf{Z}}_{\bar{\ell}-1}], \qquad \mathbf{L}_{\mathbf{Z}}^{(d_1,d_2)} = [\mathbf{0}_{d_1,d_2}, \dots, \mathbf{0}_{d_1,d_2}, \alpha_{\bar{\ell}-1}\mathbf{Z}_{\bar{\ell}}] \tag{A4}$$

where $\mathbf{Z}$ is a generic matrix placeholder, with $\widehat{\mathbf{Z}}_{\bar{\ell}-1} = \mathbf{Z}_{\bar{\ell}-1} + \beta_{\bar{\ell}-1}\mathbf{Z}_{\bar{\ell}}$, $\widehat{\mathbf{Z}}_{\bar{\ell}-2} = \mathbf{Z}_{\bar{\ell}-2} + \delta_{\bar{\ell}-1}\mathbf{Z}_{\bar{\ell}}$ and where $\mathbf{0}_{d_1,d_2}$ denotes the zero matrix with size $d_1 \times d_2$ (if $d_1 = d_2$ we omit the second dimension). Further, we define

$$\mathbf{\Phi}^{(d)} = \begin{pmatrix} -\alpha_0 \mathbf{I}_d & & & \mathbf{0}_d \\ & -\alpha_1 \mathbf{I}_d & & \vdots \\ & & \ddots & \vdots \\ & & -\alpha_{\bar{\ell}-2}\mathbf{I}_d & \mathbf{0}_d \end{pmatrix}, \qquad \mathbf{\Xi}^{(d)} = \begin{pmatrix} -\beta_0 \mathbf{I}_d & \mathbf{I}_d & & \\ -\delta_1 \mathbf{I}_d & -\beta_1 \mathbf{I}_d & \mathbf{I}_d & \\ & \ddots & \ddots & \ddots \\ & & -\delta_{\bar{\ell}-2}\mathbf{I}_d & -\beta_{\bar{\ell}-2}\mathbf{I}_d \;\; \mathbf{I}_d \end{pmatrix} \tag{A5}$$

where $\mathbf{I}_d$ is the identity matrix of size $d \times d$. Given those building blocks we construct the matrices

$$\mathbf{W}_{\mathbf{Z}}^{(d)} = \begin{pmatrix} \mathbf{T}_{\mathbf{Z}} \\ \mathbf{\Xi}^{(d)} \end{pmatrix}, \qquad \mathbf{W}_{\mathbf{Z},0}^{(d_1,d_2)} = \begin{pmatrix} \mathbf{T}_{\mathbf{Z}} \\ \mathbf{0}_{d_1(\bar{\ell}-1),d_2\bar{\ell}} \end{pmatrix}, \qquad \mathbf{X}_{\mathbf{Z}}^{(d_1,d_2)} = \begin{pmatrix} \mathbf{L}_{\mathbf{Z}}^{(d_1,d_2)} \\ \mathbf{\Phi}^{(d_2)} \end{pmatrix}, \qquad \mathbf{X}_{\mathbf{Z},0}^{(d_1,d_2)} = \begin{pmatrix} \mathbf{L}_{\mathbf{Z}}^{(d_1,d_2)} \\ \mathbf{0}_{d_1(\bar{\ell}-1),d_2\bar{\ell}} \end{pmatrix} \tag{A6}$$

and additionally

$$\mathbf{\Upsilon}^{(d)} = \begin{pmatrix} \mathbf{0}_{d(\bar{\ell}-1),d\bar{\ell}} \\ \mathbf{\Xi}^{(d)} \end{pmatrix}, \qquad \mathbf{\Theta}^{(d)} = \begin{pmatrix} \mathbf{0}_{d,d\bar{\ell}} \\ \mathbf{\Phi}^{(d)} \end{pmatrix}. \tag{A7}$$

based on which the system of equations defined by (A2) and (A3) can be compactly written as

$$(\mathbf{P}_0 + \vartheta \mathbf{P}_1 - \mathrm{j}\omega_0 \mathbf{J}) \cdot \mathbf{z} = \mathbf{0} \tag{A8}$$

where

$$\mathbf{P}_0 = \begin{pmatrix} \mathbf{W}_{\mathbf{A}}^{(N)} & & \mathbf{K}_{\mathbf{B}}^{(N,P)} & \\ & \mathbf{W}_{-\mathbf{A}^\top}^{(N)} & \mathbf{W}_{-\mathbf{C}^\top\mathbf{S}^\top,0}^{(N,P)} & \mathbf{W}_{-\mathbf{C}^\top,0}^{(N,P)} \\ \mathbf{W}_{-\mathbf{RC},0}^{(P,N)} & & \boldsymbol{\Upsilon}^{(P)} & \mathbf{K}_{\mathbf{I}_P}^{(P,P)} \\ \mathbf{W}_{\mathbf{SC},0}^{(P,N)} & \mathbf{K}_{\mathbf{B}^\top}^{(P,N)} & \mathbf{K}_{\mathbf{Q}}^{(P,P)} & \boldsymbol{\Upsilon}^{(P)} \end{pmatrix}, \quad \mathbf{P}_1 = \begin{pmatrix} \mathbf{X}_{\mathbf{A}}^{(N,N)} & & & \\ & \mathbf{X}_{-\mathbf{A}^\top}^{(N,N)} & \mathbf{X}_{-\mathbf{C}^\top\mathbf{S}^\top,0}^{(N,P)} & \mathbf{X}_{-\mathbf{C}^\top,0}^{(N,P)} \\ \mathbf{X}_{-\mathbf{RC},0}^{(P,N)} & & \boldsymbol{\Theta}^{(P)} & \\ \mathbf{X}_{\mathbf{SC},0}^{(P,N)} & & & \boldsymbol{\Theta}^{(P)}, \end{pmatrix}, \quad \mathbf{J} = \begin{pmatrix} \mathbf{K}_{\mathbf{E}}^{(N,N)} & & & \\ & \mathbf{K}_{\mathbf{E}^\top}^{(N,N)} & & \\ & & \mathbf{0}_{P\bar{\ell}} & \\ & & & \mathbf{0}_{P\bar{\ell}} \end{pmatrix} \tag{A9}$$

and

$$\mathbf{z} = [\mathbf{r}_0^\top, \dots, \mathbf{r}_{\bar{\ell}-1}^\top, \mathbf{q}_0^\top, \dots, \mathbf{q}_{\bar{\ell}-1}^\top, \mathbf{v}_0^\top, \dots, \mathbf{v}_{\bar{\ell}-1}^\top, \mathbf{w}_0^\top, \dots, \mathbf{w}_{\bar{\ell}-1}^\top]^\top. \tag{A10}$$

References

1. Zanco A, Grivet-Talocia S, Bradde T, De Stefano M. Uniformly Stable Parameterized Macromodeling Through Positive Definite Basis Functions. *IEEE Transactions on Components, Packaging and Manufacturing Technology* 2020; 10(11): 1782–1794.

2. Bradde T, Grivet-Talocia S, Toledo P, et al. Fast Simulation of Analog Circuit Blocks Under Nonstationary Operating Conditions. *IEEE Transactions on Components, Packaging and Manufacturing Technology* 2021; 11(9): 1355-1368.

3. Willems JC. Dissipative dynamical systems part I: General theory. *Archive for Rational Mechanics and Analysis* 1972; 45(5): 321–351.

4. Grivet-Talocia S. On driving non-passive macromodels to instability. *International Journal of Circuit Theory and Applications* 2009; 37(8): 863–886.

5. Schilders W, Vorst H, Rommes J. *Model order reduction: theory, research aspects and applications*. 13. Berlin: Springer . 2008.

6. Grivet-Talocia S. Package Macromodeling via Time-Domain Vector Fitting. *IEEE Microwave and Wireless Components Letters* 2003; 13(11): 472–474.

7. Triverio P, Grivet-Talocia S, Nakhla MS. A Parameterized Macromodeling Strategy with Uniform Stability Test. *IEEE Transaction on Advanced Packaging* 2009; 32(1): 205–215.

8. Ferranti F, Knockaert L, Dhaene T. Passivity-preserving parametric macromodeling by means of scaled and shifted state-space systems. *IEEE Transactions on Microwave Theory and Techniques* 2011; 59(10): 2394–2403.

9. Samuel ER, Knockaert L, Ferranti F, Dhaene T. Guaranteed Passive Parameterized Macromodeling by Using Sylvester State-Space Realizations. *IEEE Transactions on Microwave Theory and Techniques* 2013; 61(4): 1444–1454.

10. Kabir M, Khazaka R. Parametric macromodeling of high-speed modules from frequency-domain data using Loewner Matrix based method. In: *2013 IEEE MTT-S International Microwave Symposium Digest (MTT)*; 2013; Seattle (WA), USA: 1-4. 2–7 June

11. Ionita AC, Antoulas AC. Data-driven parametrized model reduction in the Loewner framework. *SIAM Journal on Scientific Computing* 2014; 36(3): A984–A1007.

12. Xiao YQ, Grivet-Talocia S, Manfredi P, Khazaka R. A Novel Framework for Parametric Loewner Matrix Interpolation. *IEEE Transactions on Components, Packaging and Manufacturing Technology* 2019; 9(12): 2404-2417.

13. Benner P, Grivet-Talocia S, Quarteroni A, Rozza G, Schilders W, Silveira LM. *Model Order Reduction. Volumes 1-3*. Berlin: De Gruyter . 2021

14. Grivet-Talocia S, Gustavsen B. *Passive macromodeling: Theory and applications*. New York, USA: John Wiley & Sons . 2015.

15. Boyd S, Chua LO. On the passivity criterion for LTI N-ports. *International Journal of Circuit Theory and Applications* 1982; 10(4): 323–333.

16. Moylan P, Chua L, Szeto E. When is a device passive?. *International Journal of Circuit Theory and Applications* 1982; 10(2): 151–165.

17. Wohlers MR. *Lumped and Distributed Passive Networks*. New York: Academic press . 1969.

18. Gustavsen B, Semlyen A. Enforcing Passivity for Admittance Matrices Approximated by Rational Functions. *IEEE Transaction on Power Systems Review* 2001; 16(1): 97–104.

19. Coelho CP, Phillips J, Silveira LM. A convex programming approach for generating guaranteed passive approximations to tabulated frequency-data. *IEEE Transactions on Computer-Aided Design of Integrated Circuits and Systems* 2004; 23(2): 293 - 301.

20. Grivet-Talocia S. Passivity Enforcement via Perturbation of Hamitonian Matrices. *IEEE Trans. Circuits and Systems I: Fundamental Theory and Applications* 2004; 51(9): 1755–1769.

21. Ihlenfeld LPRK, Oliveira GHC. Completion-Based Passivity Enforcement for Multiport Networks Rational Models. *IEEE Transactions on Power Delivery* 2021; 36(4): 2213-2220.

22. Gustavsen B. Passivity Enforcement by Residue Perturbation via Constrained Non-Negative Least Squares. *IEEE Transactions on Power Delivery* 2021; 36(5): 2758-2767.

23. Liang G, Ma L. Multivariate theory-based passivity criteria for linear fractional networks. *International Journal of Circuit Theory and Applications* 2018; 46(7): 1358–1371.

24. Liang G, Liu C. Positive-real property of passive fractional circuits in W-domain. *International Journal of Circuit Theory and Applications* 2018; 46(4): 893–910.

25. Ferranti F, Romano D, Antonini G. On the passivity of the quasi-static partial element equivalent circuit method. *International Journal of circuit theory and applications* 2019; 47(2): 304–319.

26. Ates M. Circuit theory approach to stability and passivity analysis of nonlinear dynamical systems. *International Journal of Circuit Theory and Applications* 2022; 50(1): 214–225.

27. Torun HM, Durgun AC, Aygün K, Swaminathan M. Causal and Passive Parameterization of S-Parameters Using Neural Networks. *IEEE Transactions on Microwave Theory and Techniques* 2020; 68(10): 4290-4304.

28. Ferranti F, Antonini G, Dhaene T, Knockaert L, Ruehli AE. Physics-Based Passivity-Preserving Parameterized Model Order Reduction for PEEC Circuit Analysis. *IEEE Transactions on Components, Packaging and Manufacturing Technology* 2011; 1(3): 399-409.

29. Grivet-Talocia S. A perturbation scheme for passivity verification and enforcement of parameterized macromodels. *IEEE Transactions on Components, Packaging and Manufacturing Technology* 2017; 7(11): 1869–1881.

30. Zanco A, Grivet-Talocia S, Bradde T, De Stefano M. Enforcing Passivity of Parameterized LTI Macromodels via Hamiltonian-Driven Multivariate Adaptive Sampling. *IEEE Transactions on Computer-Aided Design of Integrated Circuits and Systems* 2020; 39(1): 225-238.

31. De Stefano M, Grivet-Talocia S. A Multivariate Adaptive Sampling Scheme for Passivity Characterization of Parameterized Macromodels. In: *2021 IEEE 25th Workshop on Signal and Power Integrity (SPI)*; 2021; Siegen, Germany: 1-3. 10–12, May

32. Szeg G. *Orthogonal polynomials*. 23. Providence, (RI): American Mathematical Soc. . 1939.

33. Atkinson FV, Mingarelli A. *Multiparameter eigenvalue problems*. New York: Academic Press . 1972.

34. Dai L. *Singular Control Systems*. Berlin: Springer-Verlag . 1989.

35. Carracedo Rodriguez A, Gugercin S. The p-AAA algorithm for data driven modeling of parametric dynamical systems. *arXiv e-prints* 2020: arXiv–2003.

36. Zanco A, Grivet-Talocia S, Bradde T, De Stefano M. Multivariate macromodeling with stability and passivity constraints. In: *2018 IEEE 22nd Workshop on Signal and Power Integrity (SPI)*; 2018; Brest, France: 1-4. 22–25, May

37. Zanco A, Grivet-Talocia S. High-dimensional parameterized macromodeling with guaranteed stability. In: *2019 IEEE 28th Conference on Electrical Performance of Electronic Packaging and Systems (EPEPS), Montreal (Canada), 6–9 Oct.*; 2019: 1–3.

38. Grivet-Talocia S, Fevola E. Compact Parameterized Black-Box Modeling via Fourier-Rational Approximations. *IEEE Transactions on Electromagnetic Compatibility* 2017; 59(4): 1133-1142.

39. Abramowitz M, Stegun IA. *Handbook of mathematical functions with formulas, graphs, and mathematical tables*. 55. US Government printing office . 1948.

40. Scherer C, Weiland S. Linear matrix inequalities in control. *Lecture Notes, Dutch Institute for Systems and Control, Delft, The Netherlands* 2000. URL: https://www.imng.uni-stuttgart.de/mst/files/LectureNotes.pdf.

41. Trentelman H, Willems J. Every storage function is a state function. *Systems & Control Letters* 1997; 32(5): 249–259.

42. Anderson BDO, Vongpanitlerd S. *Network analysis and synthesis*. Engelwood Cliffs (NJ): Prentice-Hall . 1973.

43. Benner P, Kressner D, Mehrmann V. Skew-Hamiltonian and Hamiltonian Eigenvalue Problems: Theory, Algorithms and Applications. In: Drmac Z, Marusic M, Tutek Z., eds. *Proceedings of the Conference on Applied Mathematics and Scientific Computing*Springer Netherlands. 2005 (pp. 3–39)

44. Triverio P, Grivet-Talocia S, Nakhla MS, Canavero F, Achar R. Stability, Causality, and Passivity in Electrical Interconnect Models. *IEEE Trans. Advanced Packaging* 2007; 30(4): 795–808.

45. Dumitrescu B. Parameterization of positive-real transfer functions with fixed poles. *Circuits and Systems I: Fundamental Theory and Applications, IEEE Transactions on* 2002; 49(4): 523-526.

46. Saraswat D, Achar R, Nakhla MS. Global passivity enforcement algorithm for macromodels of interconnect subnetworks characterized by tabulated data. *IEEE Transactions on Very Large Scale Integration (VLSI) Systems* 2005; 13(7): 819-832.

47. Gustavsen B, Semlyen A. Enforcing passivity for admittance matrices approximated by rational functions. *IEEE Transactions on Power Systems* 2001; 16(1): 97-104.

48. Bradde T, Grivet-Talocia S, Zanco A, Calafiore GC. Data-Driven Extraction of Uniformly Stable and Passive Parameterized Macromodels. *IEEE Access* 2022; 10: 15786-15804. doi: 10.1109/ACCESS.2022.3147034

49. Wang Y, Zhang Z, Koh CK, Shi G, Pang GKH, Wong N. Passivity Enforcement for Descriptor Systems Via Matrix Pencil Perturbation. *IEEE Transactions on Computer-Aided Design of Integrated Circuits and Systems* 2012; 31(4): 532–545.

50. Zhang Z, Lei CU, Wong N. GHM: A generalized Hamiltonian method for passivity test of impedance/admittance descriptor systems. In: *2009 IEEE/ACM International Conference on Computer-Aided Design - Digest of Technical Papers*; 2009; San Jose (CA), USA: 767-773. 2–5, Nov.

51. Zhang Z, Wong N. Passivity Check of S-Parameter Descriptor Systems via S-Parameter Generalized Hamiltonian Methods. *IEEE Transactions on Advanced Packaging* 2010; 33(4): 1034–1042.

52. Boyd S, Balakrishnan V, Kabamba P. A bisection method for computing the H_∞ norm of a transfer matrix and related problems. *Mathematics of Control, Signals and Systems* 1989; 2(3): 207–219.

53. Benner P, Mehrmann V, Xu H. A numerically stable, structure preserving method for computing the eigenvalues of real Hamiltonian or symplectic pencils. *Numerische Mathematik* 1998; 78(3): 329–358.

54. De Cock K, De Moor B. Multiparameter Eigenvalue Problems and Shift-invariance. *IFAC-PapersOnLine* 2021; 54(9): 159–165.

55. Gantmakher FR. *The theory of matrices*. Mineola, (NY): American Mathematical Soc. . 1959.

56. Golub GH, Van Loan CF. *Matrix computations*. Baltimore, London: Johns Hopkins University Press. 3 ed. 1996.

57. Güttel S, Tisseur F. The nonlinear eigenvalue problem. *Acta Numerica* 2017; 26: 1–94.

58. Berhanu M. *The polynomial eigenvalue problem*. PhD thesis. University of Manchester, Manchester Institute for Mathematical Sciences, Manchester; 2005. URL: http://eprints.maths.manchester.ac.uk/582/1/mberhanu05.pdf.

59. Ferranti F, Knockaert L, Dhaene T. Parameterized S-Parameter Based Macromodeling With Guaranteed Passivity. *Microwave and Wireless Components Letters, IEEE* 2009; 19(10): 608–610.

60. Triverio P, Nakhla M, Grivet-Talocia S. Extraction of Parametric Circuit Models from Scattering Parameters of Passive RF Components. In: *Proc. of the 5th European Microwave Integrated Circuits Conference*; 2010; Paris: 393–396. 27 – 28, Sept.

61. Bradde T, Grivet-Talocia S, De Stefano M, Zanco A. A Scalable Reduced-Order Modeling Algorithm for the Construction of Parameterized Interconnect Macromodels from Scattering Responses. In: *2018 IEEE Symposium on Electromagnetic Compatibility, Signal Integrity and Power Integrity*; 2018; Long Beach (CA), USA: 650-655. 30 July – 3 Aug.

62. Manfredi P, Grivet-Talocia S. Rational Polynomial Chaos Expansions for the Stochastic Macromodeling of Network Responses. *IEEE Transactions on Circuits and Systems I: Regular Papers* 2020; 67(1): 225-234. doi: 10.1109/TCSI.2019.2942109

63. Sanathanan C, Koerner J. Transfer function synthesis as a ratio of two complex polynomials. *Automatic Control, IEEE Transactions on* 1963; 8(1): 56–58. doi: 10.1109/TAC.1963.1105517